

University of New Orleans

ScholarWorks@UNO

University of New Orleans Theses and
Dissertations

Dissertations and Theses

5-15-2009

Trellis Coded Modulation Schemes Using A New Expanded 16-Dimensional Constant Envelope Quadrature-Quadrature Phase Shift Keying Constellation

Milton I. Quinteros
University of New Orleans

Follow this and additional works at: <https://scholarworks.uno.edu/td>

Recommended Citation

Quinteros, Milton I., "Trellis Coded Modulation Schemes Using A New Expanded 16-Dimensional Constant Envelope Quadrature-Quadrature Phase Shift Keying Constellation" (2009). *University of New Orleans Theses and Dissertations*. 924.

<https://scholarworks.uno.edu/td/924>

This Thesis is protected by copyright and/or related rights. It has been brought to you by ScholarWorks@UNO with permission from the rights-holder(s). You are free to use this Thesis in any way that is permitted by the copyright and related rights legislation that applies to your use. For other uses you need to obtain permission from the rights-holder(s) directly, unless additional rights are indicated by a Creative Commons license in the record and/or on the work itself.

This Thesis has been accepted for inclusion in University of New Orleans Theses and Dissertations by an authorized administrator of ScholarWorks@UNO. For more information, please contact scholarworks@uno.edu.

Trellis Coded Modulation Schemes Using
A New Expanded 16-Dimensional Constant Envelope
Quadrature-Quadrature Phase Shift Keying Constellation

A Thesis

Submitted to the Graduate Faculty of the
University of New Orleans
in partial fulfillment of the
requirements for the degree of

Master of Science
in
Engineering

by

Milton I. Quinteros

B.S. University of New Orleans, 2007

May 2009

Acknowledgments

First of all, I would like to express special gratitude to my major advisor, Dr. Edit J. Kaminsky Bourgeois, for all her continuous support and invaluable guidance during my graduate studies.

I dedicate this work to God, who is the pillar of my strength, and to my lovely family. My father, Dr. Milton Quinteros, and my mother, Lcda. Mabel Cabrera, have been my inspiration and emotional support during this process.

I also would like to thank my beloved Carlita Rojas and her family for their endless care and help on my career.

Finally, I acknowledge my thesis committee members Dr. Juliette Ioup and Dr. Vesselin P. Jilkov for their constructive and valuable comments.

Table of Contents

LIST OF FIGURES.....	VI
LIST OF TABLES	VII
ABSTRACT	VIII
1. INTRODUCTION.....	1
1.1 CLASSICAL DIGITAL COMMUNICATION BACKGROUND.....	2
1.2 CONVOLUTIONAL CODING	2
1.3 CONVOLUTIONAL DECODING BY USING THE VITERBI ALGORITHM.....	4
1.3 MODULATORS AND DEMODULATORS	5
1.4 DESCRIPTION OF TRELLIS CODED MODULATION (TCM).....	6
1.4.1 TCM expansion penalty.....	7
1.4.2 TCM decoding.....	7
1.5 MULTIDIMENSIONAL SIGNAL SETS	8
1.6 DESCRIPTION OF SUBMITTED PAPERS	8
REFERENCES.....	9
2. A NOVEL EXPANDED 16-DIMENSIONAL CONSTANT ENVELOPE Q²PSK CONSTELLATION.....	11
ABSTRACT	11
2.1 INTRODUCTION.....	11
2.2 REVIEW OF Q ² PSK.....	12
2.3 REVIEW OF CONSTANT ENVELOPE Q ² PSK.....	13
2.4 THE NEW CEQ ² PSK CONSTELLATIONS.....	15
2.4.1 Cartwright's CEQ ² PSK Constellation.....	15
2.4.2 The 16-D CEQ ² PSK Constellations.....	17
2.5 THE NEW EXPANDED 16-D CEQ ² PSK CONSTELLATION	18

2.6 NONLINEAR CHANNELS	19
2.6.1 Recording Channel.....	19
2.6.2 Traveling Wave Tube (TWT) Channel	19
2.7 FUTURE WORK	20
2.8 CONCLUSIONS	20
2.9 REFERENCES.....	21
3. A TRELLIS-CODED MODULATION SCHEME WITH A NOVEL EXPANDED 16-DIMENSIONAL CONSTANT ENVELOPE	
Q²PSK CONSTELLATION.....	23
ABSTRACT	23
3.1 INTRODUCTION	23
3.2 REVIEW OF THE CONSTANT ENVELOPE Q ² PSK CONSTELLATIONS	25
3.2.1 4-D Constant Envelope Quadrature-Quadrature Phase Shift-Keying (CEQ ² PSK).....	26
3.2.1.1 Saha’s 4-D CEQ ² PSK.....	26
3.2.1.2 Cartwright’s 4-D CEQ ² PSK	27
3.2.2 Novel 16-D Expanded CEQ ² PSK Constellation	30
3.3 EXPANDED 16-D CEQ ² PSK CONSTELLATION PARTITION	31
3.4 TCM SYSTEM IMPLEMENTATION	32
3.5 TCM DECODING.....	34
3.6 RESULTS.....	35
3.6.1 Results for the Hardware Detector for Cartwright’s 4-D Q ² PSK Constellation	36
3.6.2 Distance Properties and Expected Coding Gains	37
3.6.3 TCM System Simulation Results	38
3.7 CONCLUSIONS AND FURTHER WORK.....	39
REFERENCES	40
4. SIMULATION DESIGN AND IMPLEMENTATION.....	42
4.1 GEOMETRICAL ANALYSIS OF THE CONSTELLATIONS.....	42

4.2 Q ² PSK SIGNAL MODULATOR BLOCK.....	43
4.3 FOUR-DIMENSIONAL CEQ ² PSK SIMULATIONS AND DECODERS.....	44
4.4 16-D CEQ ² PSK-TCM SYSTEM SIMULATIONS.....	46
4.4.1 Transmitter Simulink Block.....	46
4.4.2 Viterbi Algorithm Decoder in Simulink	47
5. CONCLUSIONS AND FUTURE WORK	49
APPENDICES.....	50
A.1 MATLAB FUNCTION ND (C)	50
A.2 MATLAB FUNCTION MSD(C).....	50
A.3 CONSTELLATION PARTITION OF 16-D CARTWRIGHT'S SIGNAL SET	50
A.4 CEQ ² PSK SYSTEM BLOCK DIAGRAM FOR SAHA'S CONSTELLATION.	55
A.5 OPTIMAL DEMODULATOR REFERENCED IN CHAPTER 3 FOR SAHA'S CONSTELLATION.	56
A.6 MAPPING BY SET-PARTITIONING SUBROUTINE.....	57
A.7 BRANCH METRIC CALCULATION EMBEDDED FUNCTION	58
A.8 ADD COMPARE AND SELECT SUBROUTINE ('FCN').....	59
A.9 TRACE-BACK FUNCTION	65
A.10: CONTAINED IN THE ATTACHED CD.....	66
A.11: CO-AUTHOR PERMISSION LETTERS	67
VITA.....	69

List of Figures

FIG. 1.1: BLOCK DIAGRAM OF A CONVOLUTIONAL CODER.	3
FIG. 1.2: A TRELLIS DIAGRAM REPRESENTATION FOR A CONVOLUTIONAL ENCODER WITH $K(M-1)$ STATES.	4
FIG. 1.3: GENERAL STRUCTURE OF ENCODER/MODULATOR FOR TCM.....	6
FIG. 3.1: BLOCK DIAGRAM OF THE PROPOSED OPTIMUM 4-D CEQ ² PSK DEMODULATOR FOR CARTWRIGHT'S SIGNAL CONSTELLATION.	29
FIG. 3. 2: PARTITION OF THE 16-D CONSTANT ENVELOPE Q ² PSK CONSTELLATION V.	32
FIG. 3.3: CONVOLUTIONAL ENCODER OF RATE 2/3.	32
FIG. 3.4: BLOCK DIAGRAM OF THE ENCODER/MODULATOR FOR THE PROPOSED 16-DCEQ ² PSK-TCM SYSTEM.	33
FIG. 3.6: FUNCTIONAL BLOCK OF THE DECODER FOR CEQ ² PSK-TCM SYSTEM.....	35
FIG. 3.5: EIGHT-STATE TRELLIS AND SUBSET TO BRANCH ASSIGNMENTS USED FOR OUR CEQ ² PSK-TCM SYSTEM.	35
FIG. 3.7: PROBABILITY OF BIT AND SYMBOL ERROR VS. E_b/N_o FOR OUR HARDWARE DETECTOR FOR CARTWRIGHT'S 4-D CEQ ² PSK CONSTELLATION.....	36
FIG. 3.8: BIT AND SYMBOL ERROR PROBABILITIES AS A FUNCTION OF E_b/N_o FOR CODED AND UNCODED 16-D CEQ ² PSK SYSTEMS.....	38
FIG. 4.1: SIMULINK BLOCK DIAGRAM OF A Q ² PSK MODULATOR.	43
FIG. 4.2: BLOCK DIAGRAM OF SYSTEM THAT COMPUTES THE BIT ERROR PROBABILITY FOR CARTWRIGHT'S CONSTELLATION.	44
FIG. 4.5: TRANSMITTER SIMULINK BLOCK DIAGRAM.	46
FIG. 4.6: CEQ ² PSK-TCM ENCODER SUBSYSTEM.	47
FIG. 4.7 VITERBI DECODER FOR THE 16-D CEQ ² PSK TCM SYSTEM.....	48

List of Tables

TABLE I: SAHA AND BIRDSALL'S CEQ ² PSK SYMBOLS	15
TABLE II: DISTANCE DISTRIBUTION OF CEQ ² PSK	15
TABLE III: CARTWRIGHT'S CEQ ² PSK SYMBOLS	17
TABLE IV: DISTANCE DISTRIBUTION OF THE 16-D CEQ ² PSK CONSTELLATIONS $\{S_{16A1}\}$ OR $\{S_{16B1}\}$	18
TABLE V: PARTIAL DISTANCE DISTRIBUTION BETWEEN SETS $\{S_{16A1}\}$ AND $\{S_{16B1}\}$ (ONLY THOSE DIFFERENT FROM THE SEDS LISTED IN TABLE IV)	19
TABLE I: THE 4-D CEQ ² PSK POINTS	33
TABLE II: GROUPING OF THE 4-D CONSTITUENT POINTS INTO SETS OF ANTIPODAL SIGNALS	33
TABLE III: 8-D GROUPS W	34
TABLE IV: FINAL GROUPING OF THE 16-D CEQ ² PSK SIGNALS.....	34
TABLE V: SED OF THE EXPANDED 16-D CEQ ² PSK	37
TABLE VI: SED DISTRIBUTION AFTER SET-PARTITIONING	38

Abstract

In this thesis, the author presents and analyzes two 4-dimensional Constant Envelope Quadrature-Quadrature Phase Shift Keying constellations. Optimal demodulators for the two constellations are presented, and one of them was designed and implemented by the author.

In addition, a novel expanded 16-dimensional CEQ²PSK constellation that doubles the number of points without decreasing the distance between points or increasing the peak energy is generated by concatenating the aforementioned constellations with a particular method and restrictions. This original 16-dimensional set of symbols is set-partitioned and used in a multidimensional Trellis-Coded Modulation scheme along with a convolutional encoder of rate $2/3$.

Effective gain of 2.67 dB over uncoded CEQ²PSK constellation with low complexity is achieved theoretically. A coding gain of 2.4 dB with 8 dB SNR is obtained by using Monte Carlo simulations. The TCM systems and demodulators were tested under an Additive White Gaussian Noise channel by using Matlab's Simulink block diagrams.

Keywords—Multidimensional constellation, constant envelope, constellation expansion, trellis coded modulation, quadrature-quadrature phase shift keying.

1. Introduction

Digital communications is a field that studies effective transmission of information in binary sequences through a particular channel [1]. By transmitting data in discrete packages, many advantages, which have been based on an extensive mathematical theory and random process analysis, can be accomplished; these include more noise immunity than analog communication systems, more information transmitted per unit bandwidth, and low costs in the implementation of digital devices.

One of the most important challenges for communications engineers is to design optimal systems that can protect transmitted messages from channel errors. Shannon's capacity theorem [2] proves that it is theoretically possible to achieve reliability in the transmission of an information sequence throughout a linear Gaussian channel by using coding.

The author of this thesis presents a system that tries to overcome the detrimental effects of a Gaussian channel by using a trellis-coded modulation (TCM) system along with a novel expanded 16-D Constant Envelope Quadrature-Quadrature Phase Shift Keying (CEQ²PSK) constellation. Therefore, the probability of an error event of the coded 16-D CEQ²PSK TCM scheme will decrease in comparison to the uncoded 16-D CEQ²PSK schemes (Saha's or Cartwright's constellations). Because the proposed TCM system has constant envelope, this scheme can be used effectively in non-linear channels such as the magnetic recording channel.

In this introductory chapter, an exposition of the fundamental theory involved in the TCM schemes is surveyed. Convolutional coding and decoding, modulators, demodulators, trellis coded modulation, and multidimensional signaling are the topics that the author presents in

this chapter. To continue, a brief description of the two first chapters which are publications¹ of the TCM system proposed, and which the author worked along on with Dr. Edit J. Kaminsky Bourgeois, Dr. Kenneth Cartwright, and Ricardo Gallegos, is given. After that, Chapter four gives the simulation design in order to present the strategy that the author used to implement the system. Finally, conclusions and future work are given at the end of this thesis.

1.1 Classical Digital Communication Background

The basic idea of transmitting discrete chunk of data is summarized in the following process: First, the information produced by a source is converted into a sequence of binary digits; this process is called source encoding or data compression [1]. After the information has been converted, the sequence of bits is passed to the channel encoder which helps the receiver to overcome the effects of noise interference encountered in the channel. At the output of the channel encoder, the binary sequence is passed to the digital modulator which maps the binary information sequence into signal waveforms. Then the signal is sent to the transmission channel. Finally, the signal reaches the destination and, a receiver catches the signal. A digital demodulator, channel decoder, and source decoder complete the steps for the transmission process of the digital data. In TCM, the modulation and encoding are performed jointly.

1.2 Convolutional Coding

Convolutional coding and decoding are the fundamental building blocks of the author's trellis modulation scheme. According to [3] the convolutional encoder generates redundant symbols as a function of a span of preceding information symbols. A convolutional encoder consists of an L-stage shift register with the outputs of the selected stages being added modulo-2 to form the encoded symbols. Figure 1.1 shows a block diagram for a convolutional coder.

¹ See references [11] and [12].

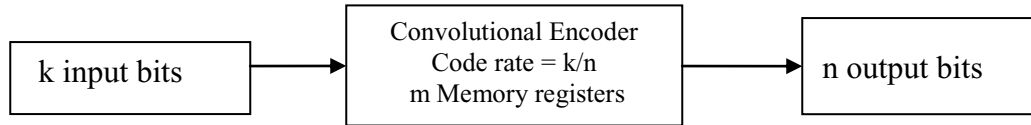


Fig. 1.1: Block diagram of a convolutional coder.

The convolutional encoder takes a block of information of k bits and generates n bits, where $n > k$. The additional $n-k$ bits are derived from the information bits, and can be used to detect and correct the errors that occurred in the original bits. The parameter called rate of the code is equal to k/n .

Convolutional Coders are commonly specified by three parameters: n , k , and m , where:

n = number of output bits

k = number of input bits

m = number of memory registers

Another important parameter is the constraint length L . This parameter represents the number of bits in the encoder memory that affects the generation of the n output bits, and it is equal to $k(m-1)$.

In addition, a convolutional encoder can be seen as finite state machine that has $2^{k(m-1)}$ states [4] with the state information stored in the memory registers. Each new input information bit produces a transition from one state to another.

The convolutional encoder can be represented by a trellis diagram which shows the state transitions and the corresponding input and outputs bits. In Fig. 1.2 a general trellis diagram representation is shown, where the paths between states is denoted as (x_i/c_i) , where x_i represents the i -th input bits, and the c_i represent the c -th output encoded bits.

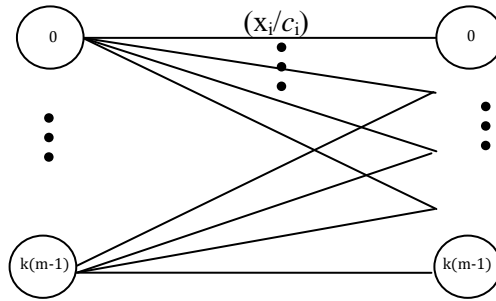


Fig. 1.2: A trellis diagram representation for a convolutional encoder with $k(m-1)$ states.

1.3 Convolutional Decoding by using the Viterbi Algorithm

The Viterbi algorithm (VA) is a computationally efficient technique for determining the most probable path through a trellis [5]. The algorithm makes a number of assumptions. First, the observed events and hidden events must each be in a sequence. Second, these two sequences must be aligned, and an observed event needs to correspond exactly to one hidden event. Third, computing the most likely hidden sequence up to certain point “ t ” must depend only on the observed event up to “ t ”.

The Viterbi decoder examines an entire received sequence of a given length (namely, decoding depth) and computes a path metric for each path in order to make a decision based on this metric. In [6], VA is claimed to be an asymptotically optimum decoding technique for convolutional codes that can determine a code signal that follows a trellis diagram.

In [7], Forney mentions that the probability of error can be made to decrease exponentially with the increasing of the constraint length or higher rates; therefore the statement suggest an improvement in the performance of the decoder, but at the cost of complexity in the design. The author of this thesis design a decoder for the convolutional encoder TCM system uses a moderated complexity which is based on a rate of $2/3$ and a constraint length of 3.

1.3 Modulators and Demodulators

A digital modulator is a device that turns a digital signal into a waveform that is ready to be sent over a particular channel. In conventional multilevel (amplitude and/or phase) systems, during each modulation interval the modulator transmits b coded information bits at a time by using $M = 2^b$ distinct waveforms, one waveform for each of the M -ary possible b -bit sequence [1]. For instance, if we have a set of 8 signals, then we are transmitting at most 3 bits, and if we are broadcasting a set of 16 signals, it means that we are conveying at most 4 bits of information during that transmission. The demodulator recovers the b -bits by making an independent M -ary nearest neighbor decision on each received signal [6].

If the mapping of information is performed under constraints, then the modulator is said to have memory [1]. If there are no constraints the modulator is recognized as memory-less [1]. The modulator used in this thesis is a memory-less.

In addition to the mapping constraints, there are other important digital modulator's characteristics that the author considered in his design such as the linearity, and the dimension of these sets of modulating signals.

Some important schemes used to modulate data are Pulse Amplitude Modulation (PAM), Phase Modulation (PM), Quadrature Amplitude Modulation (QAM), Quadrature Phase Shift Keying (QPSK), Quadrature-Quadrature Phase Shift Keying(Q²PSK) [8]. All these methods have their own way to perform the modulation from bits to analog signals. The Q²PSK modulator doesn't have constant amplitude; however, if coding is performed on the input of this modulator constant amplitude can be obtained yielding Constant Envelope Q²PSK (CEQ²PSK).

The CEQ²PSK signal set is a fundamental part of the TCM system proposed in this thesis. Further details of CEQ²PSK are given in chapters 2 and 3, and the system designed and implemented in Matlab's Simulink² is given in chapter 4.

1.4 Description of Trellis Coded Modulation (TCM)

TCM is a joint coding and modulation technique for digital transmission that is especially appropriated for band-limited channels, and it has become very popular during recent years because of the gains achieved without compromising bandwidth efficiency [6]. The key idea of TCM schemes is that modulation and coding are combined in order to map the information bits to a modulated constellation signal set; therefore, if the signal waveforms in the set that represent an information sequence are clearly separated in their Euclidian distances, then a lower error rate can be accomplished. A functional diagram of a standard TCM system is depicted in Fig. 1.3.

The TCM diagram shows that m bits are encoded to produce $m+p$ coded bits (z_m, \dots, z_{m+p}) that select a subset from the partitioned signal constellation. In addition, uncoded bits (b_0, \dots, b_{k-m+1}) select a point within the selected subset, $s(t)$, which is the final signal transmitted.

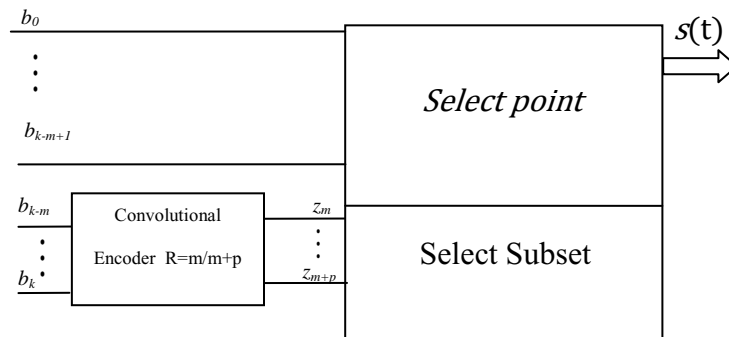


Fig. 1.3: General structure of encoder/modulator for TCM

² Matlab[™] is a registered trademark of the Math Works, Inc.

TCM systems require proper set partitioning of the constellation signal set; this task can be accomplished very easily if we have few points and the dimensionality of the signal is small. Ungerboeck [6] proposed certain rules for set partitioning 2-D signals, and Wei expanded this for multidimensional signal set [9].

Trellis coding uses dense signal sets but restrict the sequences that can be used. This provides a gain in free distance and the code imposes a time dependency on the allowed signal sequences that allows the receiver to ride through “noise burst” as it is estimating the transmitted sequence [6].

1.4.1 TCM expansion penalty

TCM schemes require more signal points compared to uncoded constellations. For instances, Ungerboeck [6] went from a 4-PSK uncoded system that transmits 2 b/s to a expanded four state Trellis Code 8-PSK modulation and conveys the same bit rate. Indeed, these additional points may be obtained at the cost of either increasing the energy in the system, or reducing the MSED of the constellation.

Kaminsky presented in [10] an X8 constellation that can be expanded without increasing the energy of the system and without reducing the MSED of the uncoded constellations. The author of this thesis follows the same procedure to expand an uncoded 16-D CEQ²PSK constellation.

1.4.2 TCM decoding

Because TCM used a convolutional encoder, a VA is used to search the most likely coded information sequence embedded in a path of the trellis. In [1], TCM decoding is suggested to be

performed in two steps. The first step corresponds to the subset decoding which is find the most likely point in each transition (the closest point in Euclidian distance), and to store the point and the shortest Euclidian distance. The second step of the decoding procedure is to use the previous Euclidian distances to find the most likely path through the trellis by using the VA.

1.5 Multidimensional Signal Sets

A set of signal waveforms can be represented geometrically as a point in N-dimensional space. For instance, binary orthogonal signals are represented geometrically as points in the two-dimensional space, and Q^2 PSK signal set form a four dimensional signal space by using two data shaping pulses and two carriers which are pair wise [8].

In addition, multidimensionality can be implemented as sequence of constituent one-, two- or four-dimensional signals [6]. For example, Kaminsky [10] achieved eight dimensions by transmitting four sequences of a 2-D 4-PSK signal set.

1.6 Description of Submitted Papers

Chapter 2 is an article published in the 2008 IEEE Region 5 BASICS conference Proc. [11]. It introduces a new set of symbols that is valid for a 4-D CEQ^2 PSK modulation system. Equally important, this chapter also introduces a novel expanded 16-D CEQ^2 PSK constellation be used in Chapter 3 for a TCM system without constellation expansion penalty.

Chapter 3 is a companion paper submitted to IEEE Globecom 2009 [12] that introduces an optimal decoder for Cartwright's CEQ^2 PSK symbols presented in Chapter 2. In addition, a proper set partition of the expanded 16-D CEQ^2 PSK constellation is given. Finally, a 16-D CEQ^2 PSK TCM system is implemented and discussed in Chapter 3.

Chapter 4 shows the implementations and simulations that generated the results presented in the papers that constituted chapters 2 and 3. Finally, conclusions of these two papers are drawn in Chapter 5, and future work is outlined.

REFERENCES

- [1] J.G Proakis, "Introduction," in *Digital Communications*, 4th edition, McGraw-Hill Science Engineering, 2000. pp 1-889.
- [2] C. E. Shannon, "A mathematical theory of communication," *Bell System Technical Journal*, vol. 27, pp. 379-423 and 623-656, July and October, 1948.
- [3] George C. Clark, Jr. and J. Bibb Cain, "Convolutional Code Structure and Viterbi Decoding," in *Error-Correction Coding for Digital Communications*, New York, Plenum Press, 1981, pp 227-238.
- [4] V. Pless, "Introduction to the Theory of Error-Correction Codes," 3rd ed. New York: John Wiley & Sons, 1998.
- [5] A. J. Viterbi, "A personal history of the Viterbi algorithm," *Signal Processing Magazine*, IEEE, vol. 23 no. 4, July 2006, pp. 120-140.
- [6] G. Ungerboeck, "Trellis-coded modulation with redundant signal sets-Part I: Introduction," *IEEE Communication Magazine*, vol. 25, no. 2, Feb 1987.
- [7] G. David. Forney, Jr., "The Viterbi Algorithm," *Proc. IEEE*, vol. 61, no. 3, pp. 268-278,

March 1973.

- [8] D. Saha and T. G. Birdsall, "Quadrature-Quadrature Phase Shift Keying," *IEEE Trans. Commun.*, vol. 37, no. 4, pp. 437-448, May 1989.
- [9] L.-F. Wei, "Trellis-Coded Modulation with Multidimensional Constellations," *IEEE Trans. Inf. Theory*, vol. IT-33, no. 4, pp. 483-501, July 1987.
- [10] E. J. Kaminsky, "Trellis coding and adaptive estimation in dually polarized systems", Ph. D. thesis, Tulane University, New Orleans, LA, June 1991.
- [11] M. I. Quinteros, K. V. Cartwright, E. J. Kaminsky, and R. U. Gallegos, "A Novel Expanded 16-Dimensional Constant Envelope Q2PSK Constellation," in 2008 IEEE Region 5 BASICS2 Conf. Proc., Kansas City, MO, pp. 1-4, Apr 2008.
- [12] M. I. Quinteros, K. V. Cartwright, E. J. Kaminsky, "A Trellis-Coded Modulation Scheme with a Novel Expanded 16-Dimensional Constant Envelope Q2PSK Constellation" submitted in IEEE Globecom 2009 Conf. Proc., Honolulu, Hawaii, 2009, pp. 6, Dec 2009.

2. A Novel Expanded 16-Dimensional Constant Envelope Q²PSK Constellation

Milton I. Quinteros, Edit J. Kaminsky, Kenneth V. Cartwright, Ricardo U. Gallegos

Abstract

We introduce a 16-dimensional constant-amplitude constellation that is generated by concatenating either four constant envelope quadrature-quadrature phase shift keying (CEQ²PSK) symbols from Saha and Birdsall or four CEQ²PSK symbols recently discovered by Cartwright and also introduced here. Our new constellation doubles the number of points available for data transmission without decreasing the distance between points or increasing energy, and may therefore be used in a trellis coded modulation (TCM) system without constellation expansion penalty. Because the new constellation has constant envelope, the modulation scheme becomes very attractive for nonlinear channels such as the magnetic recording channel or the satellite channel with traveling wave tube amplifiers.

2.1 Introduction

Considerable research effort has been devoted to developing modulation schemes that can overcome the challenges of bandwidth limited channels. Saha and Birdsall [1], [2] suggested an efficient use of available dimensions to improve the spectral efficiency of a communications system. They presented quadrature-quadrature phase shift keying (Q²PSK) and constant envelope Q²PSK (CEQ²PSK). Q²PSK is a 4-dimensional (4-D) scheme that uses two quadrature carriers and two data shaping pulses.

Constant envelope is desirable in nonlinear channels; it avoids the variations in phase produced by changing amplitude, which in turn has detrimental effects in the performance of coherent demodulators. CEQ²PSK achieves constant envelope at the expense of bandwidth efficiency because the information rate is $3/(2T)$ for CEQ²PSK while it is $2/T$ for non-constant Q²PSK. Fortunately, however, CEQ²PSK also provides a gain of 1.44 dB over non-constant Q²PSK as shown in [5], which corrects the more optimistic value of 1.76 dB given in [1].

In this paper, we present a new set of eight 4-D points which is also a valid CEQ²PSK constellation. Furthermore, we also introduce a new 16-D constellation of 8192 points with constant envelope. Our 16-D constellation is created by the union of the set produced by transmitting four of the original CEQ²PSK or four of our new CEQ²PSK points over four consecutive time intervals.

The rest of this paper is organized as follows: we present a brief review of Q²PSK and CEQ²PSK in Sections 2.2 and 2.3, respectively. In section 2.4, we introduce the new CEQ²PSK constellation discovered by Cartwright and our new expanded 16-D constellation. In section 2.5, we briefly discuss a couple of nonlinear channels in which our modulation system could be used. Suggestions for further work are given in Section 2.6. Concluding remarks are given in Section 2.7 with the main references following.

2.2 Review of Q²PSK

Quadrature-quadrature phase shift keying (Q²PSK) [1], [2] is a spectrally efficient modulation scheme that uses available signal space dimensions in a more efficient way than two dimensional schemes such as quadrature phase shift keying (QPSK) and minimum shift keying (MSK). Saha and Birdsall's scheme uses four available dimensions created by two data shaping pulses and two

quadrature carriers. The Q²PSK modulating signal set $\{s_i(t)\}$, $i = 1, \dots, 4$, is made up of the following four orthogonal waveforms:

$$s_1(t) = \cos(\pi t/2T)\cos(2\pi f_c t), |t| \leq T \quad (1a)$$

$$s_2(t) = \sin(\pi t/2T)\cos(2\pi f_c t), |t| \leq T \quad (1b)$$

$$s_3(t) = \cos(\pi t/2T)\sin(2\pi f_c t), |t| \leq T \quad (1c)$$

$$s_4(t) = \sin(\pi t/2T)\sin(2\pi f_c t), |t| \leq T. \quad (1d)$$

The carrier frequency, f_c , should be $n/4T$ where $n \geq 2$ and T is the time duration of 2 bits. The original binary data stream is demultiplexed into four signals $\{a_i(t)\}$, $i = 1, \dots, 4$, each of duration $2T$. Each $a_i(t)$ is then multiplied by the modulating signal $s_i(t)$, and the resulting signals are added to form the modulated non-constant envelope signal $S_q(t)$ [1]:

$$S_q(t) = \sum_{i=1}^4 a_i(t)s_i(t). \quad (2)$$

The number of possible symbols in this modulation technique is $2^4 = 16$ because there are four bits input to the modulator. The bit rate at the input of the modulator is $2/T$ which is twice the bit rate of the QPSK scheme.

2.3 Review of Constant Envelope Q²PSK

Constant envelope, desired for non-linear channels, can be introduced to produce CEQ²PSK, as presented in [1]. The modulated Q²PSK signal of (2) may be rewritten as:

$$S_q(t) = A(t)\cos(2\pi f_c t + \theta(t)), \quad (3)$$

where $\theta(t)$ can be any of the four possible values: $\pm 45^\circ$, $\pm 135^\circ$. This phase shift produces discontinuities in phase, and abrupt $\pm 90^\circ$ or $\pm 180^\circ$ phase changes in the Q²PSK signal may occur at a symbol transition [2].

$A(t)$ in (3) is the carrier amplitude given in [1] as:

$$A(t) = \left(2 + (a_1 a_2 + a_3 a_4) \sin \frac{\pi t}{T} \right)^{1/2}, \quad (4)$$

where $\{a_i\}$, $i = 1, \dots, 4$, are, respectively, the binary values of the input signals $\{a_i(t)\}$, $i = 1, \dots, 4$, at time t , $(n-1)T \leq t \leq nT$ (i.e., ± 1). In order to accomplish constant envelope, the amplitude $A(t)$ in (4) must fulfill the following condition [1], [2]:

$$a_1 a_2 + a_3 a_4 = 0. \quad (5)$$

For CEQ²PSK modulation we have three information input bits $\{a_i\}$, $i = 1, 2, 3$, while the fourth bit is produced by a simple block encoder of rate 3/4 where $a_4 = -a_1 a_2 / a_3$ to satisfy (5). The eight possible symbols that Saha and Birdsall found are shown in Table I, and labeled C_i , $i = 1, 2, \dots, 8$.

The set of points $\{C_i\}$, $i = 1, 2, \dots, 8$, has peak energy of 2 per 2-D (or 4 over 4-bit interval), and the minimum squared Euclidian distance (MSED) between any pair of signal points is 8.

In Table II, we show the distribution of squared distances between points in Saha and Birdsall's CEQ²PSK constellation. Obviously, the eight points at distance zero are between a point and itself.

Table I: Saha and Birdsall's CEQ²PSK symbols

		a_1	a_2	a_3	a_4
symbols	C_1	1	1	1	-1
	C_2	1	1	-1	1
	C_3	1	-1	1	1
	C_4	1	-1	-1	-1
	C_5	-1	-1	-1	1
	C_6	-1	-1	1	-1
	C_7	-1	1	-1	-1
	C_8	-1	1	1	1

Table II: Distance distribution of CEQ²PSK

Squared Euclidian distance	Number of points
0	8
8	48
16	8

2.4 The New CEQ²PSK Constellations

The main contributions of this paper are contained in this Section. We present first a second set of valid 4-D CEQ²PSK points in subsection 2.4.1. In subsection 2.4.2, we show the two 16-D constant envelope constellations, and in subsection 2.4.3 we introduce the expanded 16-D constellation which contains 8192 points, twice as many as needed to transmit 3 information bits per 4-D.

2.4.1 Cartwright's CEQ²PSK Constellation

We have found a new set of 8 symbols that is also valid for CEQ²PSK. The new set $\{K_i\}$, $i = 1, 2, \dots, 8$, has the same energy as the set $\{C_i\}$, $i = 1, 2, \dots, 8$, and the same distribution of squared distances. Therefore, our constellation also has an MSED of 8.

Table III shows the novel eight symbols. Clearly, the constant envelope condition of (5) is satisfied by this new set, and the symbol energy is the same as that of the original set shown in Table I.

However, there is another constraint that a CEQ²PSK constellation must satisfy that is not mentioned by Saha and Birdsall [1], namely,

$$a_1^2 + a_3^2 = a_2^2 + a_4^2. \quad (6)$$

The validity of (5) and (6) is established by substituting (1) into (2) to get

$$S_q(t) = \left(a_1 \cos\left(\frac{\pi t}{2T}\right) + a_2 \sin\left(\frac{\pi t}{2T}\right) \right) \cos 2\pi f_c t + \left(a_3 \cos\left(\frac{\pi t}{2T}\right) + a_4 \sin\left(\frac{\pi t}{2T}\right) \right) \sin 2\pi f_c t. \quad (7)$$

Clearly, the amplitude of (7) is given by

$$A(t) = \left[\left(a_1 \cos\left(\frac{\pi t}{2T}\right) + a_2 \sin\left(\frac{\pi t}{2T}\right) \right)^2 + \left(a_3 \cos\left(\frac{\pi t}{2T}\right) + a_4 \sin\left(\frac{\pi t}{2T}\right) \right)^2 \right]^{0.5}. \quad (8)$$

Simplifying (8) gives

$$A(t) = \left[\frac{a_1^2 + a_2^2 + a_3^2 + a_4^2}{2} + \left(\frac{a_1^2 + a_3^2}{2} - \frac{a_2^2 + a_4^2}{2} \right) \cos\left(\frac{\pi t}{T}\right) + (a_1 a_2 + a_3 a_4) \sin\left(\frac{\pi t}{T}\right) \right]^{0.5}. \quad (9)$$

Clearly, (9) has constant envelope if (5) and (6) are satisfied, as they are for the constellation of Saha and Birdsall [1] and the new one introduced here in Table III. ((9) reduces to (4) for both constellations).

Table III: Cartwright's CEQ²PSK symbols

		a_1	a_2	a_3	a_4
symbols	K_1	0	$\sqrt{2}$	$\sqrt{2}$	0
	K_2	0	$-\sqrt{2}$	$-\sqrt{2}$	0
	K_3	0	$-\sqrt{2}$	$\sqrt{2}$	0
	K_4	0	$\sqrt{2}$	$-\sqrt{2}$	0
	K_5	$\sqrt{2}$	0	0	$\sqrt{2}$
	K_6	$\sqrt{2}$	0	0	$-\sqrt{2}$
	K_7	$-\sqrt{2}$	0	0	$\sqrt{2}$
	K_8	$-\sqrt{2}$	0	0	$-\sqrt{2}$

2.4.2 The 16-D CEQ²PSK Constellations

In [3], a constellation of $2n$ -dimensional ($2n$ -D) points was proposed by transmitting n consecutive 2D in-phase and quadrature-phase pairs. A similar approach is followed here, where in order to obtain the expanded 16-dimensional constant envelope Q²PSK constellation, we use 4 consecutive 4-D CEQ²PSK symbols, instead of using 8 consecutive 2D QPSK symbols.

If four consecutive 4-D symbol time slots are taken at once, a 16-dimensional symbol can be generated. We have two subsets with symbols of the form $S_{16a} = [C_i C_j C_p C_q]$, and $S_{16b} = [K_i K_j K_q K_p]$, where $i, j, p, q = 1, 2, \dots, 8$. For the standard CEQ²PSK over 4 consecutive time intervals, there are $8^4 = 4096$ possible points $\{S_{16ai}\}$, $i = 1, 2, \dots, 4096$. The set $\{S_{16bi}\}$, $i = 1, 2, \dots, 4096$, contains the 4096 points formed by four consecutive points of Cartwright's CEQ²PSK of Table III. Table IV shows the squared distance distribution for either of these two sets. Because each 16-dimensional set has 4096 signals, the distribution has a total of $(4096)^2$ distances.

Within the set $\{S_{16ai}\}$ or $\{S_{16bi}\}$, $i = 1, 2, \dots, 4096$, the MSED between any pair of different points is still 8, and the peak energy is still equal to 2 per 2-D.

2.5 The New Expanded 16-D CEQ²PSK Constellation

Our novel 16-dimensional constellation is the union of the set $\{S_{16ai}\}$ and $\{S_{16bi}\}$, yielding $2 \cdot 8^4 = 8192$ possible points. Notice that this is not equivalent to the 4-fold Cartesian product constellation of $\{C_i\} \cup \{K_i\}$ because the four consecutive 4-D symbols used to produce the 16-D symbols must come only from one or the other 4-D constellation. This affects the partitioning that will be needed for trellis coded modulation (TCM) using our expanded constellation.

The MSED between points of this new expanded constellation is still 8, which is the intra-set MSED of each of the two 16-D sets. The MSED across sets $\{S_{16ai}\}$ and $\{S_{16bi}\}$ is equal to $8(1+(\sqrt{2}-1)^2) = 9.373$. This new constellation, then, has twice as many points within the same 16-D space, with the same energy per point, without decreasing the MSED. This will allow a TCM system to be developed that uses the expanded constellation without paying the usual constellation expansion penalty.

Table V shows the squared distances from points in $\{S_{16ai}\}$ to points in $\{S_{16bi}\}$, and the multiplicity of these. The complete squared-distance distribution for our expanded constellation is the union of those listed in Tables IV and V, with twice the number of pairs indicated; for example, there are 196608 points at MSED 8 and 131072 pairs of points with SED 9.373.

Table IV: Distance distribution of the 16-D CEQ²PSK constellations $\{S_{16ai}\}$ or $\{S_{16bi}\}$

Squared Euclidian distance	Number of pairs
0	4096
8	98304
16	901120
24	3833856
32	7102464
40	3833856
48	901120
56	98304
64	4096

Table V: Partial distance distribution between sets $\{S_{16ai}\}$ and $\{S_{16bi}\}$ (only those different from the SEDs listed in Table IV)

Squared Euclidian distance	Number of pairs
9.373	65536
15.029	524288
20.686	1835008
26.343	3670016
32.00	4587520
37.656	3670016
43.313	1835008
48.970	524288
54.627	65536

2.6 Nonlinear Channels

Because nonlinear channels require constant envelope signals, our new constellation is a good option in channels such as the recording magnetic channel and the travelling wave tube (TWT) channel. For this reason, we discuss very briefly these two channels.

2.6.1 Recording Channel

The digital magnetic recording channel is nonlinear due to a process called saturation magnetic recording [6]. This particular phenomenon has been modeled by using a Volterra series expansion.

Sands and Cioffi [7] suggest a system transfer function by using Discrete Volterra Series (DVS). According to Sands and Cioffi, the channel can be modeled with most of the nonlinear distortion represented with third-order terms, which allows for a relatively compact channel description. Signals for the recording channels should be DC-free and have constant envelope.

2.6.2 Traveling Wave Tube (TWT) Channel

The model of nonlinear TWT amplifiers presented by Saleh in [8] may be used for the satellite communications channel if the satellite amplifiers are being driven near the saturation point.

Constant amplitude modulation schemes such as the one presented in this paper allows operation of the amplifier in that situation, avoiding loss of power.

2.7 Future Work

Because our new expanded 16-dimensional has redundant symbols, we can use this constellation along with a convolutional encoder to produce a novel multidimensional trellis coded modulation (TCM) system similar to those in [3], [4], but using CEQ²PSK instead of QPSK and therefore gaining an additional advantage due to the better utilization of the signal dimensions. In order to accomplish this task, an adequate set partition has to be implemented.

Simulations of the CEQ²PSK TCM system with our expanded 16-D constellation are being conducted and shall be presented in a companion paper. The hardware detector of [5] must be modified to optimally decode the new sets. The performance of the 16-D CEQ²PSK-TCM system over nonlinear channels such as those mentioned in Section 2.5 must be determined.

2.8 Conclusions

We have proposed a second set of 4-D constant envelope quadrature-quadrature PSK (CEQ²PSK) signals comparable to those of Saha and Birdsall. Furthermore, we have used both of these CEQ²PSK sets to create a novel 16-D constellation of 8192 points. The 16-D constellation is the union of all points formed by 4 consecutive 4-D points from one or the other CEQ²PSK constellation. Our expanded 16-D constant envelope constellation allows redundancy to be introduced through a convolutional encoder in a TCM scheme without suffering any power penalty due to constellation expansion, as the MSED and the average energy of the expanded constellation are the same as those of the system before expansion: the number of symbols is

doubled without decreasing MSED or increasing power. Because this constellation has constant envelope, it is attractive for use in nonlinear channels. Optimal yet simple hardware detection is possible.

2.9 References

- [1] D. Saha and T. G. Birdsall, "Quadrature-Quadrature Phase Shift Keying," *IEEE Trans. Commun.*, vol. 37, no. 4, pp. 437-448, May 1989.
- [2] D. Saha and A. Arbor, "Quadrature-quadrature phase shift keying," *U.S. Patent 4 730 344*, March 8, 1988.
- [3] E. J. Kaminsky, J. Ayo, and K. V. Cartwright, "TCM Without Constellation Expansion Penalty," *IKCS/IEEE J. Communications and Networks*, vol. 4, no. 2, pp. 90-96, June 2002.
- [4] E. J. Kaminsky, *Trellis coding and adaptive estimation in dually polarized systems*, Ph. D. dissertation, Dept. Elect. Eng., Tulane University, New Orleans, LA, June 1991.
- [5] K. V. Cartwright, and E. J. Kaminsky, "An optimum hardware detector for constant envelope quadrature-quadrature phase-shift keying (CEQ²PSK)," in *IEEE Global Telecommunications Conference, 2005, GLOBECOM '05*, vol.1, 28 Nov 2 to Dec 2005, pp. 393-396.
- [6] R. Potter, "Digital magnetic recording theory," *IEEE Trans. Magn.*, vol. 10, no. 3, Sep 1974, pp. 502-508.
- [7] N. P. Sands and J. M. Cioffi, "Nonlinear channel models for digital magnetic recording," *IEEE Trans. Magn.*, vol. 29, no. 6, part 2, pp. 3996-3998, Nov 1993.

- [8] A. Saleh, "Frequency-Independent and Frequency-Dependent Nonlinear Models of TWT Amplifiers," *IEEE Trans. Comm.*, vol. COM-29, no. 11, pp.1715-1720, Nov 1981.

3. A Trellis-Coded Modulation Scheme with A Novel Expanded 16-Dimensional Constant Envelope Q²PSK Constellation³

Milton I. Quinteros, Edit J. Kaminsky, Kenneth V. Cartwright

Abstract

This paper presents a TCM scheme that uses a new expanded 16-Dimensional Constant Envelope Q²PSK constellation along with a simple convolutional encoder of rate 2/3. An effective gain of 2.67 dB over uncoded CEQ²PSK is achievable with low complexity and without suffering from constellation expansion penalty. Larger coding gains are easily achieved with encoders of higher rates. In addition, an optimal hardware implementation of the required decoders is described.

3.1 Introduction

Trellis-coded modulation schemes with multidimensional signals allow for performance improvement over classical two-dimensional constellations. For example, in [1], [2] it was claimed that TCM systems with lattices of four-, eight-, or 16- dimensions achieve decent coding gains of 2 dB, 3 dB, or 6 dB, respectively, over two-dimensional signals but with a loss due to constellation expansion. Indeed, the disadvantage of the constellation expansion required to introduce coding redundancy in standard TCM is the reduction of the minimum squared

³ M. I. Quinteros, K. V. Cartwright, E. J. Kaminsky, "A Trellis-Coded Modulation Scheme with a Novel Expanded 16-Dimensional Constant Envelope Q²PSK Constellation" submitted in IEEE Globecom 2009 Conf. Proc., Honolulu, Hawaii, 2009, pp. 6, Dec 2009.

Euclidian distance (MSED) between points for a given energy level, or the increase of modulation level and energy for a given MSED [3].

In [4], Saha and Arbor reported a set of signals that uses two data shaping pulses and two carriers which are pair-wise quadrature in phase to create a spectrally efficient four dimensional (4-D) signal set called Quadrature-Quadrature Phase Shift-Keying (Q²PSK).

Acha and Carrasco [5] and Saha [6] utilize Saha's standard 4-D Q²PSK constellation for their TCM systems along with convolutional encoders of different rates. These schemes, however, achieve some gains at the cost of data rate. In addition to the rate cost paid for using these schemes, and the care required in order to avoid catastrophic error propagation [5], some of the Q²PSK trellis codes proposed by Saha, Acha and Carrasco do not have constant envelope. Their constant envelope TCM systems are obtained by further reducing the data rate by half.

During recent years, some work has been done in design of multidimensional signal sets that allow TCM to be implemented without constellation expansion penalty [3], [7], i.e., without increasing the modulation level. Kaminsky, Ayo and Cartwright's multidimensional TCM schemes of [3] are based on QPSK signals of even dimensions of eight and above. This family of constant envelope constellations is generated by concatenating n QPSK points or n QPSK points rotated by 45 degrees ($n \geq 4$) without any constellation expansion loss. In [7], a 16-D signal set with constant envelope was generated by concatenating four CEQ²PSK signals from Saha's or four CEQ²PSK signals from Cartwright's 4-D constellation. Therefore, the same idea of [3] is followed in [7] to introduce redundancy for coding without increasing the modulation level while preserving average and peak energies constant.

Here, we use the constellation we proposed in [7] to implement a simple multidimensional TCM system that uses a convolutional encoder of rate $2/3$ to achieve an asymptotic coding gain of 3 dB over uncoded CEQ²PSK. Because nonlinear channels require constant envelope signals, this 16-D CEQ²PSK-TCM system is a good option in channels that require non-linear power amplifiers. Larger coding gains are easily achieved with this constellation by using higher-rate encoders.

Additionally, a hardware detector (based on the demodulator described in [8]) for the 4-D CEQ²PSK discovered by Cartwright is proposed here. The complete implementation of the TCM system is also given.

The rest of this paper is organized as follows: In Section 3.2, a review of CEQ²PSK constellations and their decoders –including presentation of our new hardware detector for Cartwright’s CEQ²PSK – is presented. Section 3.3 presents the set-partitioning into eight sets required for the novel 16-D expanded CEQ²PSK constellation. Section 3.4 discusses the TCM system implementation, and Section 3.5 reports the development of the TCM decoder. Results, including Monte Carlo simulations of the system proposed in this paper are presented and discussed in Section 3.6. Finally, in Section 3.7, conclusions are drawn and future work is mentioned, followed by references.

3.2 Review of the Constant Envelope Q²PSK Constellations

In this section we discuss separately the two 4-dimensional constant envelope Q²PSK constellations, and the expanded 16-dimensional Q²PSK constellation.

3.2.1 4-D Constant Envelope Quadrature-Quadrature Phase Shift-Keying (CEQ²PSK)

In what follows, we review Saha's original 4-D CEQ²PSK [9] and the 4-D CEQ²PSK, discovered by Cartwright [7]. An optimal decoder for the former was presented in [8] and a similar hardware decoder for the latter is proposed here.

3.2.1.1 Saha's 4-D CEQ²PSK

Quadrature-Quadrature Phase Shift-keying (Q²PSK) and Constant Envelope Q²PSK (CEQ²PSK) signal sets were introduced by Saha and Birdsall in [9].

The four dimensional non-constant envelope Q²PSK may be defined as

$$S_q(t) = \sum_{i=1}^4 a_i(t)s_i(t), \quad (1)$$

where the four signals $\{a_i(t)\}$, $i = 1, \dots, 4$, each of duration $2T$, are the original binary data streams, and the modulating signal set $\{s_i(t)\}$, $i = 1, \dots, 4$, is defined as follows [9]:

$$s_1(t) = \cos(\pi t/2T)\cos(2\pi f_c t), |t| \leq T \quad (2a)$$

$$s_2(t) = \sin(\pi t/2T)\cos(2\pi f_c t), |t| \leq T \quad (2b)$$

$$s_3(t) = \cos(\pi t/2T)\sin(2\pi f_c t), |t| \leq T \quad (2c)$$

$$s_4(t) = \sin(\pi t/2T)\sin(2\pi f_c t), |t| \leq T. \quad (2d)$$

The carrier frequency, f_c , should be $n/(4T)$ where $n \geq 2$, and T is the time duration of 2 bits.

In order to obtain constant envelope, Saha and Birdsall introduced an encoder of rate 3/4 that accepts three information serial input streams $\{a_1(t), a_2(t), a_3(t)\}$, and generates a code word

$\{a_1(t), a_2(t), a_3(t), a_4(t)\}$ such that the first three bits in the codeword are the information bits and the fourth is an odd parity check bit [9]. Therefore, the eight possible transmitted signals for the original CEQ²PSK are $S_1 = [a, a, b, -b]$ and $S_2 = [a, -a, b, b]$, where a, b are either +1 or -1 [8]. It is also mentioned in [9] that CEQ²PSK is achieved at the expense of the information transmission rate which is reduced from $2/T$ to $3/(2T)$.

To obtain the maximum achievable performance of CEQ²PSK an optimal detector is needed. In [8], Cartwright and Kaminsky presented a CEQ²PSK hardware detector that reaches the performance of CEQ²PSK predicted in [9]. This decoder uses five hard-limiters, four adders, four absolute value circuits, two inverters, and a decision function that activates a trigger for a four-pole double-throw switch.

3.2.1.2 Cartwright's 4-D CEQ²PSK

In [7], a new set of eight 4-D symbols that is also valid for CEQ²PSK was introduced. This new set has the same energy and distribution of squared distances as the original CEQ²PSK constellation from [9]. Cartwright's symbols may be defined by an orthogonal transformation of Saha's constant envelope symbols. Let R^4 be the 4-D rotational operation [10]:

$$R^4 = \begin{bmatrix} R & 0 \\ 0 & R \end{bmatrix}, \quad (3)$$

where R is

$$R = \begin{bmatrix} \cos(45^\circ) & -\sin(45^\circ) \\ \sin(45^\circ) & \cos(45^\circ) \end{bmatrix}. \quad (4)$$

Because the eight possible transmitted 4-D signals for Cartwright's constellations are generated by rotating the component 2-D signals, the new CEQ²PSK points, S_{1r} and S_{2r} , corresponding to Saha's S_1 and S_2 are:

$$S_{1r} = R^4 S_1, \quad (5)$$

$$S_{2r} = R^4 S_2, \quad (6)$$

or $S_{1r} = [0, \sqrt{2}a, \sqrt{2}b, 0]$ and $S_{2r} = [\sqrt{2}a, 0, 0, \sqrt{2}b]$, where a, b are either +1 or -1. The proof that these eight symbols are also valid for CEQ²PSK is given in [7].

We now discuss the implementation of the optimal hardware detector for Cartwright's constellation. Fig. 3.1 depicts the block diagram of our proposed detector which closely resembles the receiver in [8], but uses a different decision function $F(\cdot)$, gains of magnitude $\sqrt{2}$, and requires four multipliers which may be implemented as electronic switches, if so desired.

The received signal $r(t)$ is the transmitted signal $s(t)$ corrupted by additive white Gaussian noise (AWGN) $n(t)$ with power spectral density N_0 :

$$r(t) = s(t) + n(t) \quad (7)$$

The block $F(\cdot)$ in Fig. 3.1 calculates \hat{d} as in (8):

$$\hat{d} = \frac{1}{2} [\text{sgn}(w - y) + 1], \quad (8)$$

and therefore determines the estimated symbol $\hat{S} = [\hat{a}_1, \hat{a}_2, \hat{a}_3, \hat{a}_4]$. The values of w and y are given by (9) and (10), respectively:

$$w = |a_{1r}| + |a_{4r}|, \quad (9)$$

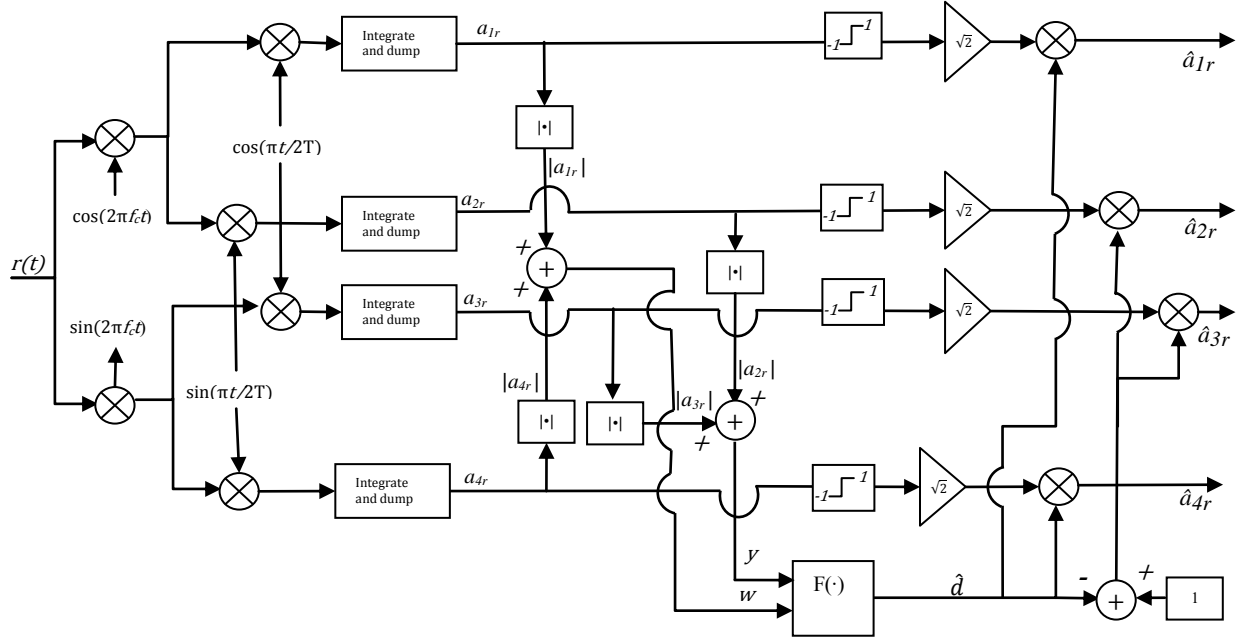


Fig. 3.1: Block diagram of the proposed optimum 4-D CEQ²PSK demodulator for Cartwright's signal constellation.

$$y = |a_{2r}| + |a_{3r}|, \quad (10)$$

and $\{a_{ir}\}$, $i = 1, \dots, 4$ are the outputs of the correlation detectors.

If a member of S_{1r} is transmitted, $y = 2\sqrt{2}$ and $w = 0$, but when a member of S_{2r} is transmitted, $w = 2\sqrt{2}$ and $y = 0$. Therefore, when a member of S_{1r} has been transmitted $w < y$ and $\hat{d} = 0$, but when $w > y$, a member of the S_{2r} has been transmitted and $\hat{d} = 1$. The output symbol, then, is obtained from (9):

$$\hat{S} = \hat{d}\hat{S}_{2r} + (1 - \hat{d})\hat{S}_{1r}. \quad (11)$$

Our optimum hardware decoder is a direct implementation of

$$\hat{a}_{1r} = \sqrt{2} \operatorname{sgn}(a_{1r}) \hat{d} \quad (12a)$$

$$\hat{a}_{2r} = \sqrt{2} \operatorname{sgn}(a_{2r}) (1 - \hat{d}) \quad (12b)$$

$$\hat{a}_{3r} = \sqrt{2} \operatorname{sgn}(a_{3r}) (1 - \hat{d}) \quad (12c)$$

$$\hat{a}_{4r} = \sqrt{2} \operatorname{sgn}(a_{4r}) \hat{d}, \quad (12d)$$

which follows from (11). In order to verify the performance of the demodulator, Monte Carlo simulations were performed and compared with the optimum hardware detector published in [8]; these results are presented in Section 3.6.

3.2.2 Novel 16-D Expanded CEQ²PSK Constellation

If four consecutive 4-D points from either Saha's or Cartwright's CEQ²PSK constellation are taken together, a 16-D signal is obtained. In this way, two sets of 4096 16-D symbols each, S_a for Saha's or S_b for Cartwright's, are formed.

The expanded constellation, V , is defined as the union of these two constellations:

$$V = \{S_a \cup S_b\}. \quad (13)$$

Our expanded 16-D CEQ²PSK signal set is therefore formed in a way similar to Kaminsky, Ayo and Cartwright's expanded constellation of [3], but with different constituent signal points. Peak energy, average energy, and minimum squared Euclidian distance (MSED) is maintained while doubling the size of the constellation, so this set of 16-D symbols is obtained without any constellation expansion penalty. Because the four consecutive 4-D symbols must come from one or the other 4-D CEQ²PSK constellation, the set-partition for the TCM system cannot be performed exactly as is done when the expanded constellation is formed by the Cartesian product of the constituent constellations, as in [1]. In the next Section we present the set partition for the 16-D expanded constellation V .

3.3 Expanded 16-D CEQ²PSK Constellation Partition

TCM schemes require a proper set-partitioning of the constellation in order to increment the free distance of the code. In this section we show how the constellation V is partitioned into the eight subsets required by our simple TCM encoder. We use $\{A_i\}_{i=1, \dots, 4}$ to denote the four subsets formed from S_a and $\{B_i\}_{i=1, \dots, 4}$ for the 16-D CEQ²PSK points from S_b . The MSED within V is 8, but the intra-subset MSED within $\{A_i\}$ or $\{B_i\}$ is increased to 16. This allows us to achieve an asymptotic gain of 3 dB with just 8 subsets and a simple 8-state convolutional encoder of rate 2/3. To achieve larger gains, further partitioning is needed, along with a trellis with more states.

First, each family S_a and S_b is partitioned independently by using the method of Wei [1], as follows: The 4-D constituent points of the set S_a (the eight original CEQ²PSK signals of Saha [9]) $\{S_1 \cup S_2\}$ can be partitioned into eight sublattices named 1,2,4,8,14,13,11,7 (to correspond to their binary values). The same is true for $\{S_{1r} \cup S_{2r}\}$, the constituent 4-D points of the set S_b , but the eight sublattices are named $1_r, 2_r, 4_r, 8_r, 14_r, 13_r, 11_r, 7_r$. Now we have 16 4-D sublattices with MSED of 8; these are shown in Table I.

Next, we group these 16 4-D sublattices into 8 groups of antipodal signals. These groups are called Q_i for Saha's and Q_{ir} for Cartwright's signals, and $i = 1, \dots, 4$. Table II shows these groups. At this point, we have reduced the number of sublattices from 16 to 8, and we have increased the MSED within Q_i and Q_{ir} to 16. Each Q group has two 4-D signals.

We now form the 8-D types by concatenating two 4-D Q_i or two 4-D Q_{ir} to obtain 32 8-D types with MSED of 8. These 32 types are defined as $Q_{ij} = [Q_i, Q_j]$ and $Q_{ijr} = [Q_{ir}, Q_{jr}]$, $i, j = 1, \dots, 4$. We now proceed to group the Q_{ij} and Q_{ijr} into eight 8-D sets W_i and W_{ir} of 16 points each, such that the intra-set MSED is equal to 16. This grouping is shown in Table III.

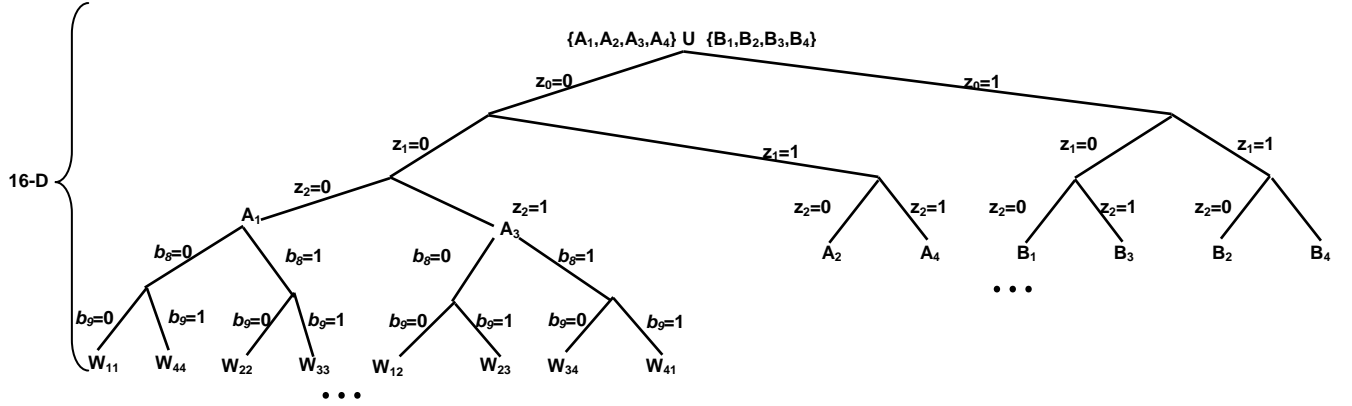


Fig.3. 2: Partition of the 16-D Constant Envelope Q^2PSK constellation V .

To proceed further, from the W types we construct the 16-D sublattices by concatenating two 8-D types: $W_{ij} = [W_i, W_j]$, and $W_{ijr} = [W_{ir}, W_{jr}]$, $i, j = 1, \dots, 4$. These 32 16-D sublattices have MSED of 16 and 256 points each.

Finally, these 16-D W_{ij} and W_{ijr} sublattices are grouped into the eight subsets $\{A_k\}, \{B_k\}$, $k = 1, \dots, 4$. Table IV shows how the W_{ij} and W_{ijr} are grouped. These subsets still have MSED of 16, contain 1024 points each, and they are required for the TCM system that uses a convolutional encoder of rate $2/3$. Fig. 3.2 shows a tree diagram of the set partitioning.

3.4 TCM System Implementation

Our multidimensional TCM system uses one of Ungerboeck's feedback convolutional encoders from [11]. It has rate $2/3$ and constraint length 3 and is shown in Fig. 3.3. Remember that our TCM system has a CEQ²PSK modulator over four consecutive modulation time intervals, each of duration $2T$.

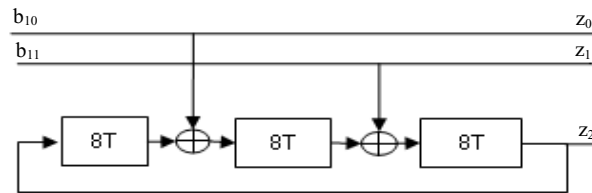


Fig. 3.3: Convolutional encoder of rate $2/3$.

Fig. 3.4 depicts the complete 16-D CEQ²PSK-TCM system. Two of the 12 bits of information, (b_{10}, b_{11}) , arriving every four signaling intervals enter the convolutional encoder to produce three coded bits (z_0, z_1, z_2) . The output of the convolutional encoder selects one of the eight subsets obtained in Section III, A_k or B_k . Two other uncoded bits (b_8, b_9) select one of the W_{ij} or W_{ijr} types from within the selected group. Fig. 3.2 shows the mapping of these five bits to some of the 16-D subsets.

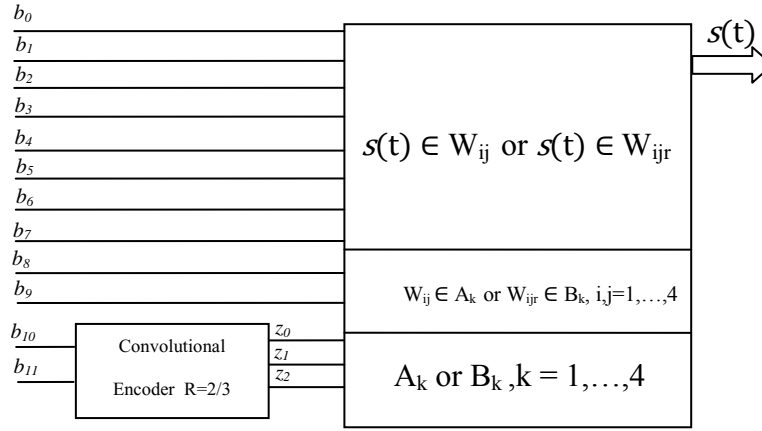


Fig. 3.4: Block diagram of the encoder/modulator for the proposed 16-DCEQ²PSK-TCM system.

Table I: The 4-D CEQ²PSK points

$S_1 \cup S_2$	Saha's	$S_{1r} \cup S_{2r}$	Cartwright's			
1	-1 -1 -1 1	1_r	0	$-\sqrt{2}$	$-\sqrt{2}$	0
2	-1 -1 1 -1	2_r	0	$-\sqrt{2}$	$\sqrt{2}$	0
4	-1 1 -1 -1	4_r	$-\sqrt{2}$	0	0	$-\sqrt{2}$
8	1 -1 -1 -1	8_r	$\sqrt{2}$	0	0	$-\sqrt{2}$
14	1 1 1 -1	14_r	0	$\sqrt{2}$	$\sqrt{2}$	0
13	1 1 -1 1	13_r	0	$\sqrt{2}$	$-\sqrt{2}$	0
11	1 -1 1 1	11_r	$\sqrt{2}$	0	0	$\sqrt{2}$
7	-1 1 1 1	7_r	$-\sqrt{2}$	0	0	$\sqrt{2}$

Table II: Grouping of the 4-D constituent points into sets of antipodal signals

Saha's Q	Cartwright's Q_r
$Q_1 = \{1; 14\}$	$Q_{1r} = \{1_r; 14_r\}$
$Q_2 = \{2; 13\}$	$Q_{2r} = \{2_r; 13_r\}$
$Q_3 = \{4; 11\}$	$Q_{3r} = \{4_r; 11_r\}$
$Q_4 = \{8; 7\}$	$Q_{4r} = \{8_r; 7_r\}$

Table III: 8-D groups W

Saha's W	Cartwright's W_r
$W_1 = \{Q_{11}; Q_{22}; Q_{33}; Q_{44}\}$	$W_{1r} = \{Q_{11r}; Q_{22r}; Q_{33r}; Q_{44r}\}$
$W_2 = \{Q_{12}; Q_{23}; Q_{34}; Q_{41}\}$	$W_{2r} = \{Q_{12r}; Q_{23r}; Q_{34r}; Q_{41r}\}$
$W_3 = \{Q_{13}; Q_{24}; Q_{31}; Q_{42}\}$	$W_{3r} = \{Q_{13r}; Q_{24r}; Q_{31r}; Q_{42r}\}$
$W_4 = \{Q_{14}; Q_{21}; Q_{32}; Q_{43}\}$	$W_{4r} = \{Q_{14r}; Q_{21r}; Q_{32r}; Q_{43r}\}$

Table IV: Final grouping of the 16-D CEQ²PSK signals

Saha's A	Cartwright's B
$A_1 = \{W_{11}; W_{22}; W_{33}; W_{44}\}$	$B_1 = \{W_{11r}; W_{22r}; W_{33r}; W_{44r}\}$
$A_2 = \{W_{12}; W_{23}; W_{34}; W_{41}\}$	$B_2 = \{W_{12r}; W_{23r}; W_{34r}; W_{41r}\}$
$A_3 = \{W_{13}; W_{24}; W_{31}; W_{42}\}$	$B_3 = \{W_{13r}; W_{24r}; W_{31r}; W_{42r}\}$
$A_4 = \{W_{14}; W_{21}; W_{32}; W_{43}\}$	$B_4 = \{W_{14r}; W_{21r}; W_{32r}; W_{43r}\}$

Finally, the rest of the information bits (b_0 through b_7) select one of the 256 points from within the selected 16-D W_{ij} or W_{ijr} types. The selected signal $s(t)$ is transmitted. In the next Section we discuss the required decoding for the modulation scheme aforementioned.

3.5 TCM Decoding

In our TCM system, the received signals, corrupted by noise, are decoded by using a soft-decision maximum-likelihood sequence decoder [12]. We use the Viterbi decoding algorithm [13], [14] to search the trellis and find the most likely paths, given the received sequence of subsets. The trellis is shown in Fig. 3.5 with the subset assignment given in the usual top-down fashion. Because our convolutional encoder has a constraint length of 3 and rate $2/3$, a decoding depth of 24 was used in the decoder implementation [14]. Fig. 3.6 shows a simplified block diagram of the decoder used in our 16-D CEQ²PSK-TCM system. The noisy signal, $r(t)$, goes simultaneously to the decoders for Saha's and Cartwright's CEQ²PSK, but without implementing the hardlimiting operations. These soft 16-D output symbols are the input to the VA decoder.

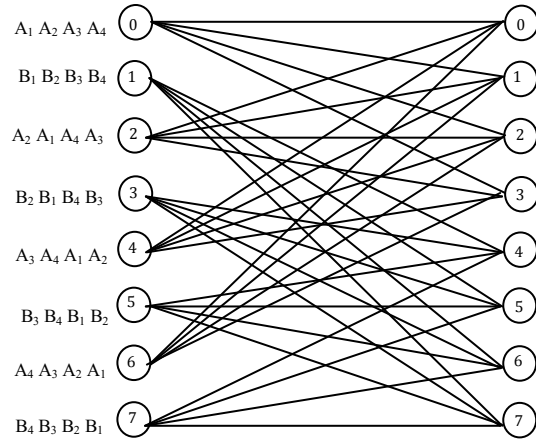


Fig. 3.5: Eight-state trellis and subset to branch assignments used for our CEQ^2PSK -TCM system.

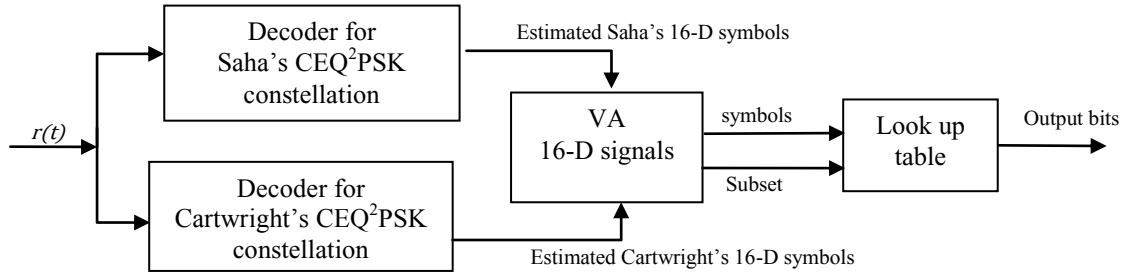


Fig. 3.6: Functional block of the decoder for CEQ^2PSK -TCM system.

The mapping from input symbols to output bits is performed as follows: First, the VA estimates the most likely of the state transitions and the corresponding subset for that transition after 24 16-D intervals of modulation; therefore, by using the state transitions and the subset, the two information bits (b_{10}, b_{11}) can be decoded.

Finally, the other 10 bits are obtained by using a look-up table of 1024 rows, corresponding to the 1024 symbols in the estimated subset.

3.6 Results

We divide this Section into three parts. First, we discuss the results of our proposed hardware detector for Cartwright's 4-D CEQ^2PSK constellation, presented in Section 3.2. Then we present

the analysis of the gains for our coded 16-D CEQ²PSK-TCM system over the uncoded reference CEQ²PSK system (S_a or S_b), and the required information about the distance distribution of the appropriate constellations. Finally, we present and briefly discuss the simulation results which corroborate our analysis.

3.6.1 Results for the Hardware Detector for Cartwright's 4-D Q²PSK Constellation

Fig. 3.7 shows the performance of our hardware detector for Cartwright's 4-D CEQ²PSK constellation in terms of probability of bit error versus bit signal to noise ratio (E_b/N_o), with E_b the energy per information bit and N_o the spectral density of AWGN. The markers indicate simulation results and the line shows the theoretical results [8]. Monte Carlo simulations for our hardware decoder were run until 50 errors were counted and match the results reported in [8] for the standard CEQ²PSK signal set detector and also match the theoretical results.

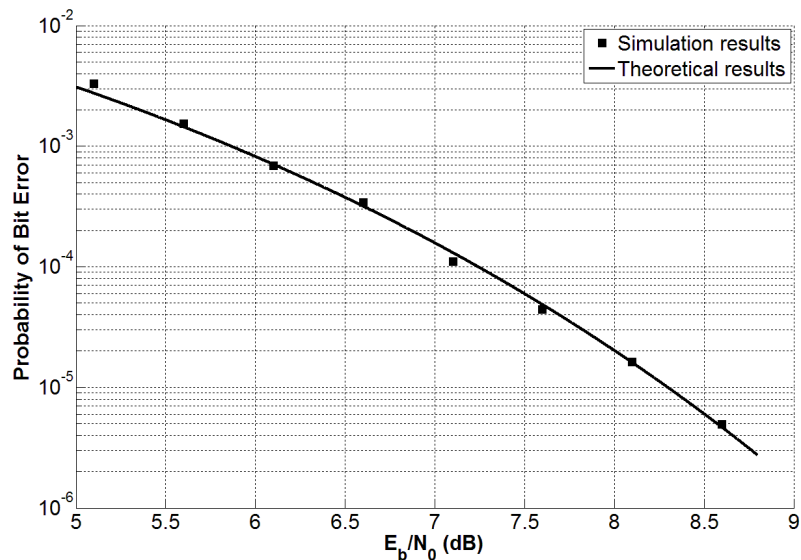


Fig. 3.7: Probability of bit and symbol error vs. E_b/N_o for our hardware detector for Cartwright's 4-D CEQ²PSK Constellation.

3.6.2 Distance Properties and Expected Coding Gains

Table V lists the smallest twelve squared Euclidian distances (SED) of the expanded CEQ²PSK constellation. Table VI shows the SED distribution of the partitioned constellation. The columns labeled d_k^2 represent the SED, and the values in the column named $N(d_k)$ are the number of points at SED d_k^2 . The MSED for the uncoded constellation (CEQ²PSK) is $d_u^2 = 8$, and has $N_u = 24$ points at that distance. The free distance of our simple TCM system is given by the parallel transitions in the trellis and is $d_c^2 = 16$ with an error coefficient (in 16-D) of $N_c = 76$. These values determine the asymptotic gain of the coded system [11], [12]:

$$G_a = 10 \log_{10} \left(\frac{d_c^2}{d_u^2} \right), \quad (14)$$

which yields to 3.01 dB because the squared free distance is doubled. However, we also have to take into consideration the loss caused by the number of neighbors at MSED [3], [10]; this loss normalized to 2-D, λ , is [8]:

$$\lambda = \frac{\log_{10} \left(\frac{N_c}{N_u} \right)}{\log_{10}(32)}, \quad (15)$$

which gives a loss of 0.33 dB for our code. The effective gain is therefore $\gamma_{eff} = G_a - \lambda = 2.67$ dB. Higher gains are possible with encoders of higher rate; the achievable asymptotic gains are also listed in Table V.

Table V: SED of the expanded 16-D CEQ²PSK

d_k^2	G_a (dB)	d_k^2	G_a (dB)
8.000	-	26.343	5.17
9.373	-	32.000	6.02
15.029	-	37.657	6.73
16.000	3.01	40.000	6.99
20.686	4.13	43.314	7.34
24.000	4.77	48.000	7.78

Table VI: SED distribution after set-partitioning

Subsets A_i or B_i	
d_k^2	$N(d_k)$
16	76
24	192
32	486
40	192
48	76
64	1

3.6.3 TCM System Simulation Results

The performance of our multidimensional TCM system was corroborated by using Monte Carlo Simulations; 20 errors are counted before the simulation stops. Fig. 3.8 shows the results in terms of bit and symbol error probabilities versus signal to noise ratio (SNR) for the reference uncoded 16-D CEQ²PSK and the trellis-coded 16-D system that uses the expanded CEQ²PSK constellation and decoding depth of 24.

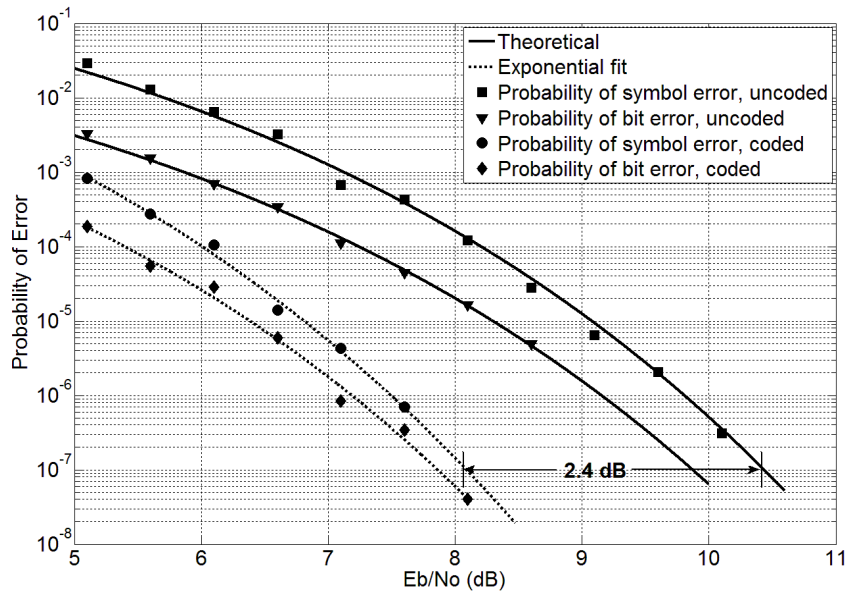


Fig. 3.8: Bit and symbol error probabilities as a function of E_b/N_o for coded and uncoded 16-D CEQ²PSK systems

Comparison of the curves corresponding to the coded and uncoded probabilities of symbol error indicates that the effective gain of 2.67 is not yet achieved at a SNR of slightly over 8 dB; the gain, however, increases with increasing SNR, and also with increasing decoding depth. The gain in bit error rate (BER) is slightly less because it cannot be guaranteed that a single bit is in error if a symbol is in error; as SNR increases, the likelihood of a single bit error per symbol error increases, so the bit and symbol probability of error curves tend to merge at large SNR.

3.7 Conclusions and Further Work

The main contribution of this paper was to show the design of a TCM system using an expanded 16-D CEQ²PSK constellation that allows the introduction of 1 bit of redundancy without constellation expansion penalty. We used a simple convolutional encoder of rate $2/3$ to achieve an effective gain of 2.67 dB while maintaining constant envelope and without reducing the bandwidth efficiency over the uncoded CEQ²PSK reference system. Considerably higher gains may be obtained with the same constellation by using more complex encoders. We also presented a hardware detector for Cartwright's 4-D Q²PSK constellation which was shown to be optimum.

Future work will include an analysis of the actual bandwidth efficiency of the system. The effects of non-linearities in the channel will be incorporated into the study, and the performance in fading channels will also be evaluated.

References

- [1] L.-F. Wei, "Trellis-Coded Modulation with Multidimensional Constellations," *IEEE Trans. Inf. Theory*, vol. IT-33, no. 4, pp. 483-501, Jul. 1987.
- [2] G. D. Forney Jr., R. G. Gallager, G. R. Lang, F. M. Longstaff, and S. U. Qureshi, "Efficient Modulation for Band-Limited Channels," *IEEE J. Select. Areas in Commun.*, vol. JSAC-2, no. 5, pp. 632-647, Sep. 1984.
- [3] E. J. Kaminsky, J. Ayo, and K. V. Cartwright, "TCM without Constellation Expansion Penalty," *J. Communications and Networks*, vol. 4, no. 2, pp. 90-96, Jun. 2002.
- [4] D. Saha and A. Arbor, "Quadrature-quadrature Phase Shift Keying," U.S. Patent 4730344, Mar. 8, 1988.
- [5] V. Acha and R. A. Carrasco, "Trellis Coded Q²PSK Signals. Part 1: AWGN and Nonlinear Satellite Channels," *IEE Proc. Commun.*, vol. 141, no. 3, pp. 151-158, Jun. 1994.
- [6] D. Saha, "Channel Coding with Quadrature-quadrature Phase Shift-Keying Signals," *IEEE Trans. Commun.*, vol. 38, no. 4, pp. 409-501, Apr. 1990.
- [7] M. I. Quinteros, K. V. Cartwright, E. J. Kaminsky, and R. U. Gallegos, "A Novel Expanded 16-Dimensional Constant Envelope Q²PSK Constellation," in 2008 *IEEE Region 5 BASICS2 Conf. Proc.*, Kansas City, MO, pp. 1-4, Apr. 2008.
- [8] K. V. Cartwright and E. J. Kaminsky, "An Optimum Hardware Detector for Constant Envelope Quadrature-quadrature Phase Shift-Keying (CEQ²PSK)," in *IEEE Globecom*

- 2005 *Conf. Proc.*, vol. 1, St. Louis, MO, 2005, pp. 393-396, Dec. 2005.
- [9] D. Saha and T. G. Birdsall, "Quadrature-Quadrature Phase Shift Keying," *IEEE Trans. Commun.*, vol. 37, no. 4, pp. 437-448, May 1989.
- [10] G. D. Forney, "Coset Codes Part 1: Introduction and Geometrical Classification," *IEEE Trans. Inf. Theory*, vol. 34, no. 5, pp. 1123-1151, Sep. 1988.
- [11] G. Ungerboeck, "Channel Coding with Multilevel/Phase Signals," *IEEE Trans. Inf. Theory*, vol. IT-28, no. 1, pp. 55-67, Jan. 1982.
- [12] G. Ungerboeck, "Trellis-Coded Modulation with Redundant Signal Sets Part I and II," *IEEE Commun. Mag.*, vol. 25, no. 2, pp. 5-21, Feb. 1987.
- [13] A. J. Viterbi, "Error Bounds for Convolutional Codes and an Asymptotically Optimum Decoding Algorithm," *IEEE Trans. Inf. Theory*, vol. IT-13, no. 2, pp. 260-269, Apr. 1967.
- [14] G. C. Clark and J. B. Cain, "Convolutional Code Structure and Viterbi Decoding," in *Error-Correction Coding for Digital Communications*, New York: Plenum Press, 1981, pp. 262-263.

4. Simulation Design And Implementation

In this chapter a survey of the systems that were implemented by using Matlab and Simulink software is covered in detail.

4.1 Geometrical Analysis of the Constellations

The author of this thesis defines in Matlab a matrix constellation:

$$C = \begin{bmatrix} r_0^1 & \dots & r_0^N \\ \vdots & \ddots & \vdots \\ r_k^1 & \dots & r_k^N \end{bmatrix}, \quad (1)$$

where the subscript represents the number of points in the signal set and the superscript is the dimensionality of the constellation. In other words, the rows represent the number of points in the constellation, and number of columns indicates the dimension. For instance, the expanded 16-D CEQ²PSK signal set matrix has 8192 rows and 16 columns.

Another important parameter is the dissimilarity matrix which contains all the combinations of the pairwise SED. For instance, for the expanded 16-D CEQ²PSK constellation the dissimilarity matrix is a square matrix of 8192 by 8192 elements.

In order to compute geometrical parameters such as SED and number of neighbors at a particular distance two Matlab subroutines were created.

Function **Nd(•)** [see Appendix A.1] computes a histogram of all possible squared Euclidian distances in a constellation matrix. The input is a matrix constellation such as defined in (1). The output of this subroutine returns two matrixes of two columns each, with the number of rows is basically determined by the number of SED that exists in a constellation signal set.

Function **msd(•)** [see Appendix A.2] computes the minimum squared Euclidian distance of a constellation matrix.

Appendix A.3 contains the program that the author coded in order to partition the expanded 16-D CEQ²PSK constellation. Only Cartwright is mentioned in Appendix A.3 because the same program applies for Saha’s constellation partition. Appendix A.3 produces several outputs, but the most important ones are B1, B2, B3, and B4 which are four of the eight subsets described in Chapter 3. In addition, a second partition is also implemented in Appendix A.3, which produces 64 subsets with MSED of 24. These 64 subsets can be coded with a convolutional encoder of rate 6/7.

4.2 Q²PSK Signal Modulator Block.

Fig. 4.1 shows a Simulink block diagram of the modulator that generates Q²PSK signals. The input of this block diagram is a sequence of bits, and the output is the modulated signal.

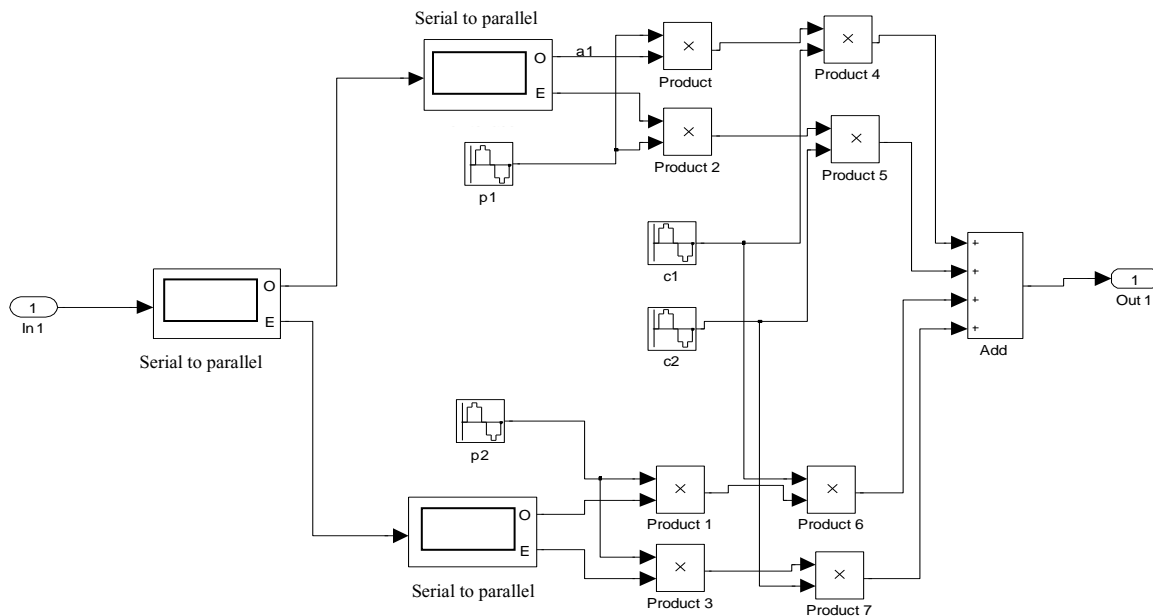


Fig. 4.1: Simulink block diagram of a Q²PSK modulator.

The blocks with a sinusoidal symbol are defined as follows:

$$p1 = \cos(\pi t/2T), \quad (2)$$

$$p2 = \sin(\pi t/2T), \quad (3)$$

$$c1 = \cos(2\pi f_c t), \quad (4)$$

$$c2 = \sin(2\pi f_c t), \quad (5)$$

where f_c is the frequency of the carrier and $2T$ is the modulation symbol time interval. These two parameters and the sampling time can be adjusted. Fig. 4.1 implements (2) from Chapter 2.

4.3 Four-Dimensional CEQ²PSK Simulations and Decoders

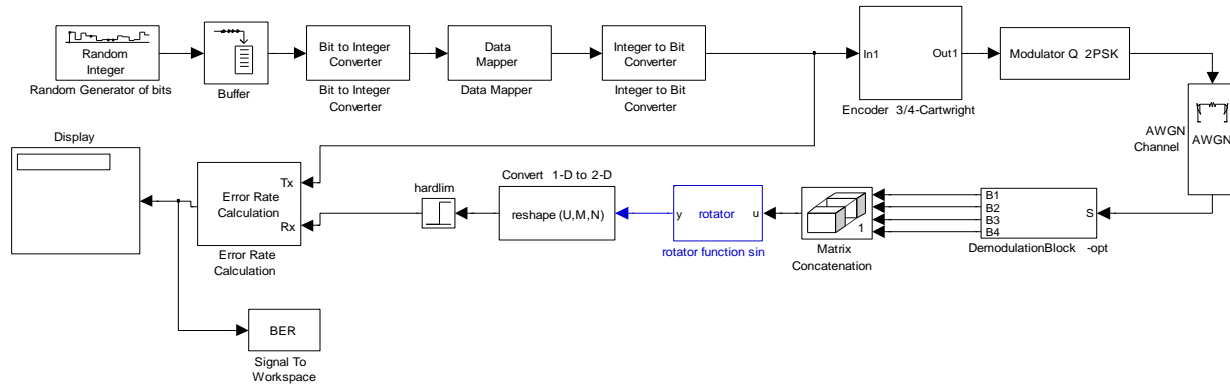


Fig. 4.2: Block diagram of system that computes the bit error probability for Cartwright's constellation.

Fig. 4.2 shows the complete system that the author implemented in order to compute probability of error for the Cartwright's 4-D CEQ²PSK constellation. The Matlab BER tool box was used in order to compute the bit error probability. The author also performed simulations for the original Saha's CEQ²PSK constellation, and these block diagrams are depicted in Appendices A.4 and A.5.

The input to the system is the random generation of 3 bits. The received symbols are output after the hardlimiter. The Error Rate calculation box compares the received bits with the transmitted and computes the bit error rate.

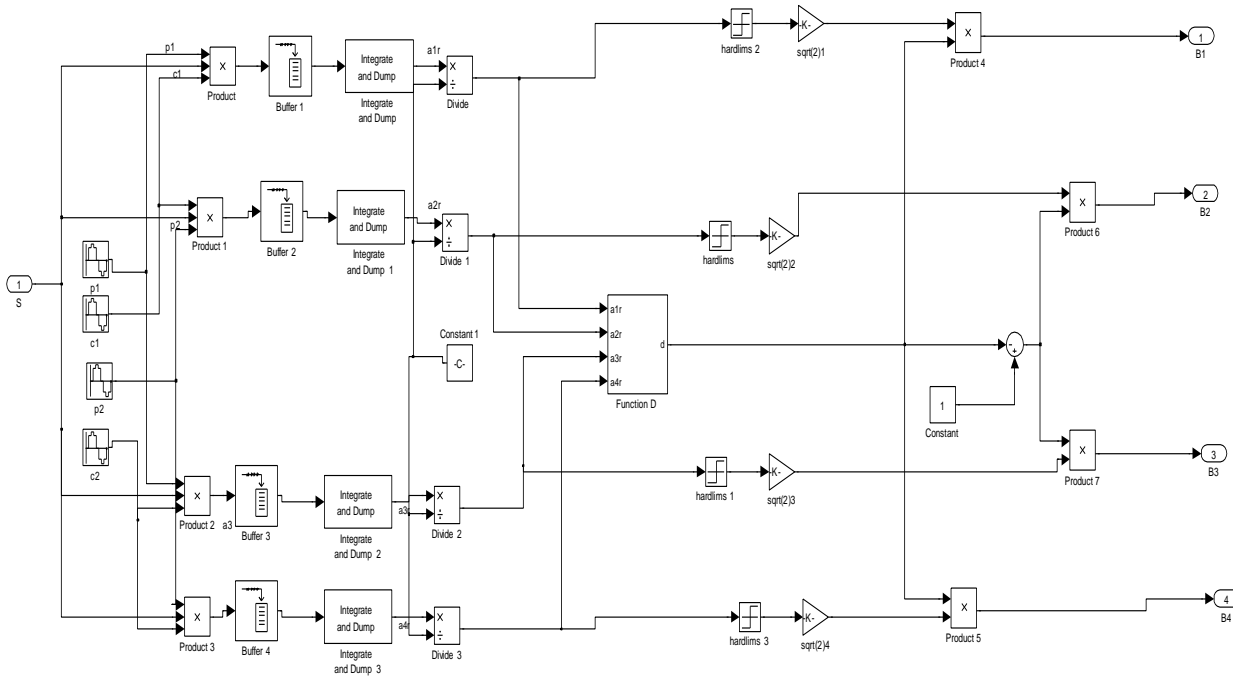


Fig. 4.3: Decoder for Cartwright's Constellation

Fig. 4.3 shows the block diagram of the demodulator for Cartwright's constellation. The block function D performs the operation described in (8) of Chapter 3 for this particular demodulator.

In order to compute the probability of symbol error, the only change needed in the system shown in Fig. 4.2 is to introduce a block that converts bits to symbol for both the transmitted bits and for the received bits.

The transmitted signal is delayed in this system because of the numerical integration, and the buffer blocks. Therefore, a block that correlates the transmitted symbols with the received

symbols (“Find Delay”) was used to compute the delays required for the Error Rate Calculation block.

4.4 16-D CEQ²PSK-TCM System Simulations

The following figure depicts the Simulink block diagram that is used to compute the probability of bit error for a 16-D CEQ²PSK-TCM system. The “Transmitter” and the “Viterbi Decoder 16D signals” blocks are described in the following subsections.

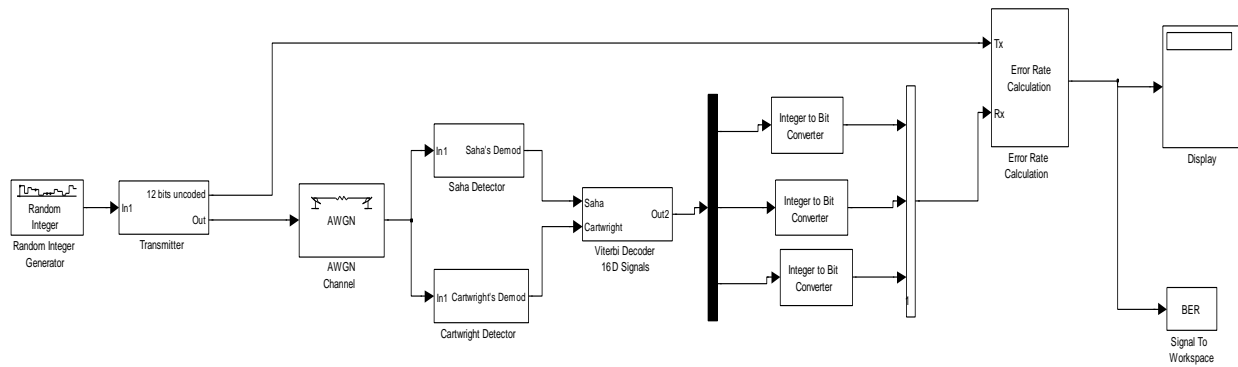


Fig. 4.4 Block diagram that computes the probability of bit error of the coded system described in Chapter 3.

4.4.1 Transmitter Simulink Block

Fig. 4.5 shows the Transmitter block diagram implanted in Simulink. This subsystem maps 12 information bits to a 16-D CEQ²PSK analog signal by using the procedure described in the Section 3.4 of Chapter 3.

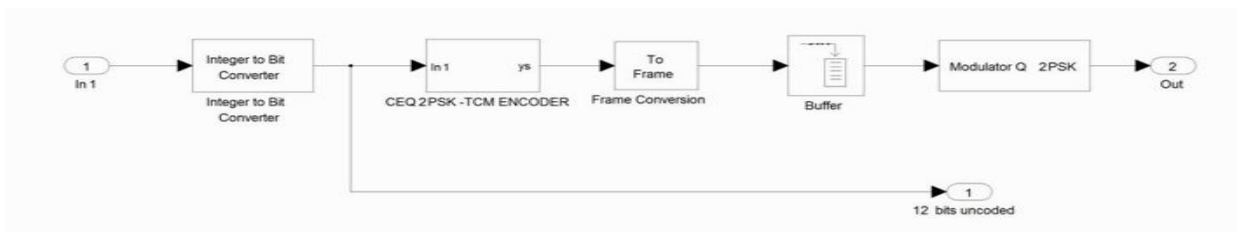


Fig. 4.5: Transmitter Simulink block diagram.

The inputs of the “CEQ2PSK-TCM ENCODER” block are 12 information bits, and the outputs are vectors of the expanded CEQ²PSK constellation. These outputs become the inputs of the Q²PSK modulator system block, so an analog signal of 16-D is transmitted. Fig. 4.6 shows a block diagram that has a convolutional encoder of rate 2/3, and the embedded Matlab subroutine (TCM Function) [see Appendix A.6].

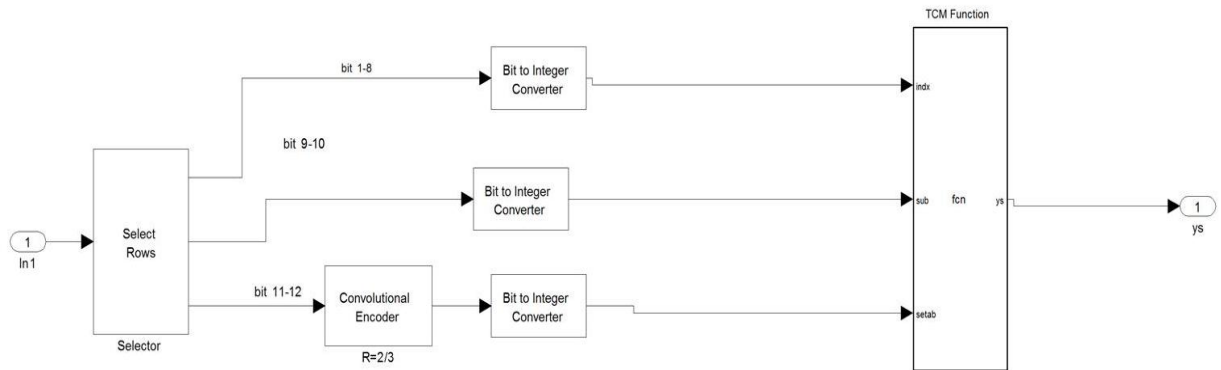


Fig. 4.6: CEQ²PSK-TCM ENCODER subsystem.

4.4.2 Viterbi Algorithm Decoder in Simulink

The software implementation of the Viterbi decoder shown in Fig. 4.4 is made of three main block components: a branch metric calculation, a function that searches for the most likely symbols in a trellis based on the 24 outputs of the branch metric calculation, and a trace-back block for the path.

All the components are shown in Fig. 4.5. The blocks are embedded functions, and the codes can be found in Appendices A.7, A.8 and A.9.

The input for the function given in Appendix A.7 is the output of the demodulator of Cartwright’s signals without hard limiters in 16-D, so it is a soft decision symbol of 16

dimensions. The same program flow for Saha's branch metric calculation, but using the input of the soft decision demodulator for Saha's signal discussed in Chapter 3.

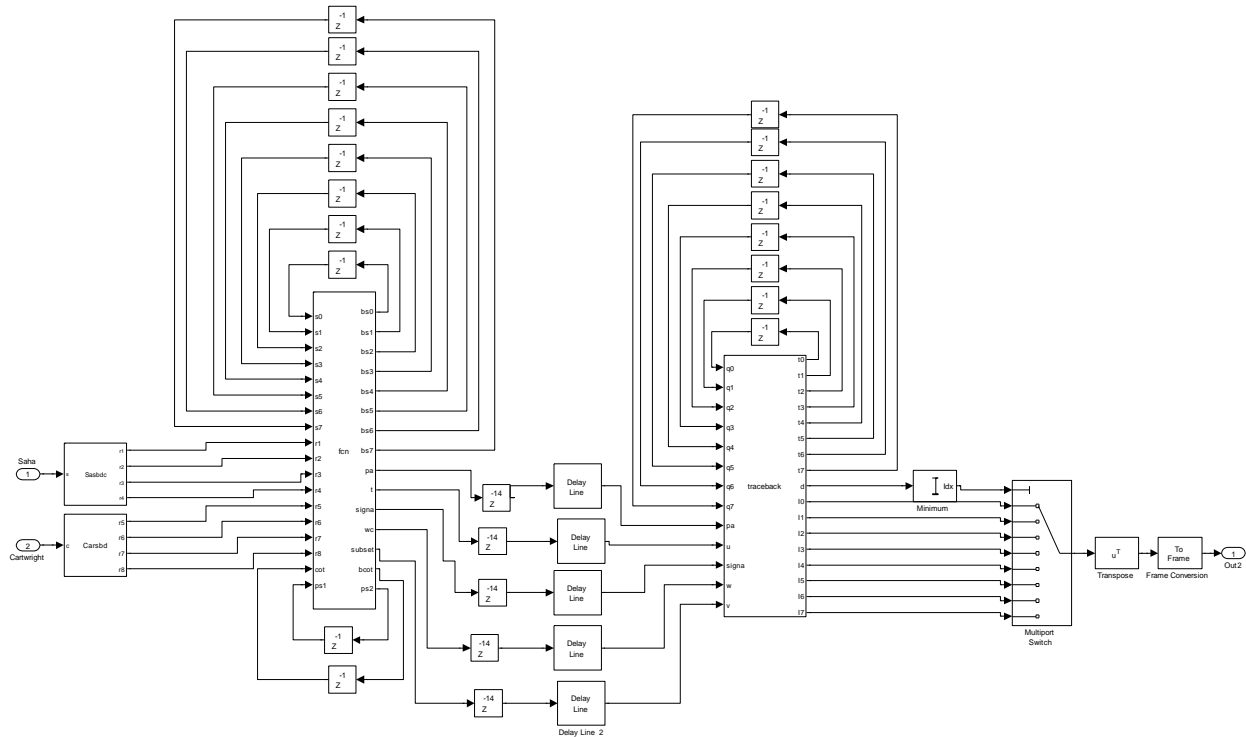


Fig. 4.7 Viterbi Decoder for the 16-D CEQ²PSK TCM system.

The Appendix A.8 is an embedded program coded by the author in Simulink that looks for the survivors paths in the trellis based on the received signal. This block receives the branch metric calculation for the two signal sets: Saha's and Cartwright's.

The Appendix A.9 is another embedded function that was coded by the author in order to restore the maximum-likelihood path from the outputs of the Appendix A.8.

Finally, in order to compute the probability of symbol, a bit-to -nteger block diagram is added at the output of the decoder.

5. Conclusions and Future Work

The 16-D CEQ²PSK TCM system presented in this thesis can achieve an asymptotic gain of 3.01 dB over uncoded 16-D CEQ²PSK. However, a penalty due to the number of neighbors produces an effective gain of 2.6 dB.

The simulation results do not reach the effective gain because of two main reasons:

- 1) The “integrate and dump” block produces a small computational error.
- 2) The SNR must be higher than 8 dB.
- 3) Second order errors affect the performances of the system.

Nevertheless, we achieved a coding gain of 2.4 dB, and this gain start to increase very slowly as the SNR increases above 8 dB.

Other systems may be implemented in order to obtain higher gains. For example, the author of this thesis found a 64 subset partition with a MSED of 24. This system will be implemented in future and is expected to yield an asymptotic gain of 4.77 dB and an effective gain of 4.57 dB. These gains are obtained because the MSED for this partition is 24 and the error coefficient is 48 at this distance.

The expanded uncoded 16-D CEQ²PSK can be used to transmit an additional bit over a non-expanded 16-D CEQ²PSK without increasing the bandwidth or the energy of the system.

Finally, the author is encouraged by these results to develop a unified theory of expanded constellations that may be used with TCM system without paying the penalty of constellation expansion.

Appendices

A.1 Matlab Function Nd (C)

```
function [R D]=Nd(C)
%The input of this function is a constellation matrix C where the size is
%mxn. The value m represents the number of points in the constellation and
%the value n the number of dimensions.
%The output R is the following: first column represents
%the squared distances of the constellation, and the second column is
%the number of pairs at particular distance
%The output D is the number of neighbors at particular squared distance

Cs=round(squareform(pdist(C).^2)*1000)/1000; %Dissimilarity matrix
rounded to three decimals
K=unique(sort(round(pdist(C).^2*1000)/1000)); %intra-set distances rounded
to three decimals
K=[0 K]; %Add the zero distance
n=hist(Cs(:),K);
R=[n' K'];
D=zeros(length(K),2);
Z=[];
for i=2:length(K)
    [I J]=find(Cs==K(i));
    D(i,1:2)=[K(i) nnz(find(J==J(1)))];
end
```

A.2 Matlab function msd(C)

```
function [d]=msd(const)
%This function calculates the mean squared distance (MSED) of a
%constellation matrix. The input is constellation matrix of mxn where m is
%the number of points, and n is the number of dimensions.
[p r]=size(const);
if p==1
    d=0;
else
    d=min(pdist(const))^2;
end
```

A.3 Constellation partition of 16-D Cartwright's signal set

```
%Generation of points and distances
clc
clear
%-----
```

```

%Cartwright's Constant Envelope Q2PSK Constellation
%These eight symbols are stored
%inside the variable Sb2

```

```

c=sqrt(2);
Sb2(:,1)=[0 c c 0 14];
Sb2(:,2)=[0 c -c 0 13];
Sb2(:,3)=[c 0 0 c 11];
Sb2(:,4)=[c 0 0 -c 8];
Sb2(:,5)=[0 -c -c 0 1];
Sb2(:,6)=[0 -c c 0 2];
Sb2(:,7)=[-c 0 0 -c 4];
Sb2(:,8)=[-c 0 0 c 7];
Sb2=Sb2';

```

```

QR1=[Sb2(1,:); Sb2(5,:)];
QR2=[Sb2(2,:); Sb2(6,:)];
QR3=[Sb2(7,:); Sb2(3,:)];
QR4=[Sb2(4,:); Sb2(8,:)];

```

```

%-----
QR11=[QR1(1,1:4) QR1(1,1:4);QR1(1,1:4) QR1(2,1:4);...
      QR1(2,1:4) QR1(1,1:4);QR1(2,1:4) QR1(2,1:4)];
FR1=[QR11(1,:);QR11(4,:)];
FR2=[QR11(2,:);QR11(3,:)];

```

```

QR12=[QR1(1,1:4) QR2(1,1:4);QR1(1,1:4) QR2(2,1:4);...
      QR1(2,1:4) QR2(1,1:4);QR1(2,1:4) QR2(2,1:4)];
FR3=[QR12(1,:);QR12(4,:)];
FR4=[QR12(2,:);QR12(3,:)];

```

```

QR13=[QR1(1,1:4) QR3(1,1:4);QR1(1,1:4) QR3(2,1:4);...
      QR1(2,1:4) QR3(1,1:4);QR1(2,1:4) QR3(2,1:4)];
FR5=[QR13(1,:);QR13(4,:)];
FR6=[QR13(2,:);QR13(3,:)];

```

```

QR14=[QR1(1,1:4) QR4(1,1:4);QR1(1,1:4) QR4(2,1:4);...
      QR1(2,1:4) QR4(1,1:4);QR1(2,1:4) QR4(2,1:4)];
FR7=[QR14(1,:);QR14(4,:)];
FR8=[QR14(2,:);QR14(3,:)];

```

```

%-----
QR21=[QR2(1,1:4) QR1(1,1:4);QR2(1,1:4) QR1(2,1:4);...
      QR2(2,1:4) QR1(1,1:4);QR2(2,1:4) QR1(2,1:4)];
FR9=[QR21(1,:);QR21(4,:)];
FR10=[QR21(2,:);QR21(3,:)];

```

```

QR22=[QR2(1,1:4) QR2(1,1:4);QR2(1,1:4) QR2(2,1:4);...
      QR2(2,1:4) QR2(1,1:4);QR2(2,1:4) QR2(2,1:4)];
FR11=[QR22(1,:);QR22(4,:)];
FR12=[QR22(2,:);QR22(3,:)];

```

```

QR23=[QR2(1,1:4) QR3(1,1:4);QR2(1,1:4) QR3(2,1:4);...
      QR2(2,1:4) QR3(1,1:4);QR2(2,1:4) QR3(2,1:4)];
FR13=[QR23(1,:);QR23(4,:)];
FR14=[QR23(2,:);QR23(3,:)];

```

```

QR24=[QR2(1,1:4) QR4(1,1:4);QR2(1,1:4) QR4(2,1:4);...
      QR2(2,1:4) QR4(1,1:4);QR2(2,1:4) QR4(2,1:4)];
FR15=[QR24(1,:);QR24(4,:)];
FR16=[QR24(2,:);QR24(3,:)];

```

```

QR31=[QR3(1,1:4) QR1(1,1:4);QR3(1,1:4) QR1(2,1:4);...
      QR3(2,1:4) QR1(1,1:4);QR3(2,1:4) QR1(2,1:4)];
FR17=[QR31(1,:);QR31(4,:)];
FR18=[QR31(2,:);QR31(3,:)];

```

```

QR32=[QR3(1,1:4) QR2(1,1:4);QR3(1,1:4) QR2(2,1:4);...
      QR3(2,1:4) QR2(1,1:4);QR3(2,1:4) QR2(2,1:4)];
FR19=[QR32(1,:);QR32(4,:)];
FR20=[QR32(2,:);QR32(3,:)];

```

```

QR33=[QR3(1,1:4) QR3(1,1:4);QR3(1,1:4) QR3(2,1:4);...
      QR3(2,1:4) QR3(1,1:4);QR3(2,1:4) QR3(2,1:4)];
FR21=[QR33(1,:);QR33(4,:)];
FR22=[QR33(2,:);QR33(3,:)];

```

```

QR34=[QR3(1,1:4) QR4(1,1:4);QR3(1,1:4) QR4(2,1:4);...
      QR3(2,1:4) QR4(1,1:4);QR3(2,1:4) QR4(2,1:4)];
FR23=[QR34(1,:);QR34(4,:)];
FR24=[QR34(2,:);QR34(3,:)];

```

```

QR41=[QR4(1,1:4) QR1(1,1:4);QR4(1,1:4) QR1(2,1:4);...
      QR4(2,1:4) QR1(1,1:4);QR4(2,1:4) QR1(2,1:4)];
FR25=[QR41(1,:);QR41(4,:)];
FR26=[QR41(2,:);QR41(3,:)];

```

```

QR42=[QR4(1,1:4) QR2(1,1:4);QR4(1,1:4) QR2(2,1:4);...
      QR4(2,1:4) QR2(1,1:4);QR4(2,1:4) QR2(2,1:4)];
FR27=[QR42(1,:);QR42(4,:)];
FR28=[QR42(2,:);QR42(3,:)];

```

```

QR43=[QR4(1,1:4) QR3(1,1:4);QR4(1,1:4) QR3(2,1:4);...

```

```

QR4(2,1:4) QR3(1,1:4);QR4(2,1:4) QR3(2,1:4)];
FR29=[QR43(1,:);QR43(4,:)];
FR30=[QR43(2,:);QR43(3,:)];

```

```

QR44=[QR4(1,1:4) QR4(1,1:4);QR4(1,1:4) QR4(2,1:4);...
QR4(2,1:4) QR4(1,1:4);QR4(2,1:4) QR4(2,1:4)];
FR31=[QR44(1,:);QR44(4,:)];
FR32=[QR44(2,:);QR44(3,:)];

```

```

WB1=[QR11; QR22; QR33; QR44];
WB2=[QR12; QR23; QR34; QR41];
WB3=[QR13; QR24; QR31; QR42];
WB4=[QR14; QR21; QR32; QR43];

```

-----16D types-----

```

WB11=concat(WB1,WB1);
WB12=concat(WB1,WB2);
WB13=concat(WB1,WB3);
WB14=concat(WB1,WB4);

```

```

WB21=concat(WB2,WB1);
WB22=concat(WB2,WB2);
WB23=concat(WB2,WB3);
WB24=concat(WB2,WB4);

```

```

WB31=concat(WB3,WB1);
WB32=concat(WB3,WB2);
WB33=concat(WB3,WB3);
WB34=concat(WB3,WB4);

```

```

WB41=concat(WB4,WB1);
WB42=concat(WB4,WB2);
WB43=concat(WB4,WB3);
WB44=concat(WB4,WB4);

```

-----Grouping 16D types-----

```

B1=[WB11; WB22; WB33; WB44];
B2=[WB12; WB23; WB34; WB41];
B3=[WB13; WB24; WB31; WB42];
B4=[WB14; WB21; WB32; WB43];

```

-----Second Partition-----

```

gr1=[FR7;FR8;FR27;FR28;FR10;FR9;FR21;FR22];
gr2=[FR19;FR20;FR16;FR15;FR30;FR29;FR2;FR1];
gr3=[FR14;FR13;FR18;FR17;FR4;FR3;FR31;FR32];
gr4=[FR25;FR26;FR6;FR5;FR23;FR24;FR11;FR12];
ARc=[FR1;FR2;FR3;FR4;FR5;FR6;FR7;FR8;FR9;FR10;FR11;FR12;FR13;FR14;FR15;FR16; .
. .

```

FR17;FR18;FR19;FR20;FR21;FR22;FR23;FR24;FR25;FR26;FR27;FR28;FR29;FR30;FR31;FR32];

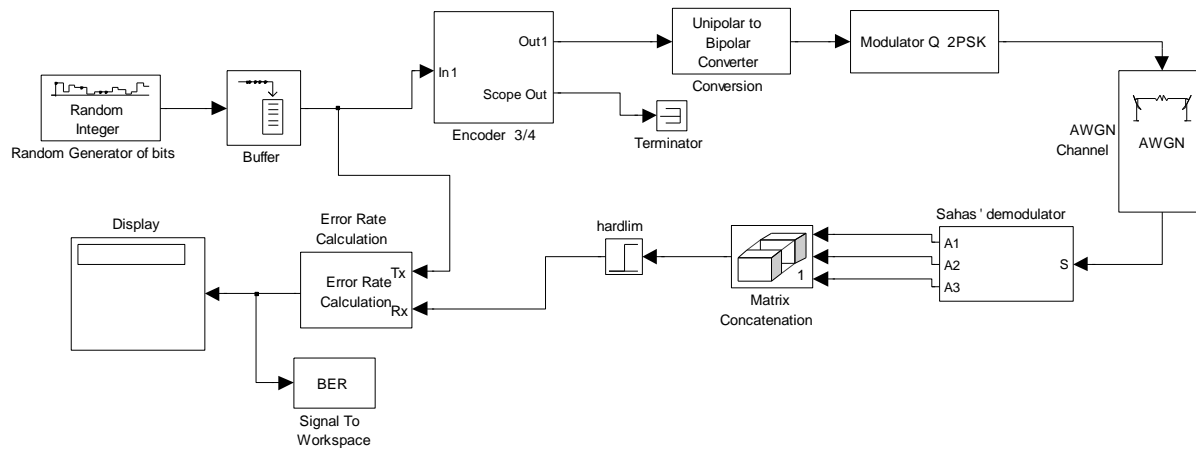
[ZR1 ZR2]=contx(Arc, [gr1;gr2;gr3;gr4]);
[ZR3
ZR4]=contx(Arc, [circshift(gr1,4);circshift(gr2,4);circshift(gr3,4);circshift(gr4,4)]);
[ZR5
ZR6]=contx(Arc, [circshift(gr1,8);circshift(gr2,8);circshift(gr3,8);circshift(gr4,8)]);
[ZR7
ZR8]=contx(Arc, [circshift(gr1,12);circshift(gr2,12);circshift(gr3,12);circshift(gr4,12)]);

[ZR9 ZR10]=contx(Arc, [gr2;gr3;gr4;gr1]);
[ZR11
ZR12]=contx(Arc, [circshift(gr2,4);circshift(gr3,4);circshift(gr4,4);circshift(gr1,4)]);
[ZR13
ZR14]=contx(Arc, [circshift(gr2,8);circshift(gr3,8);circshift(gr4,8);circshift(gr1,8)]);
[ZR15
ZR16]=contx(Arc, [circshift(gr2,12);circshift(gr3,12);circshift(gr4,12);circshift(gr1,12)]);

[ZR17 ZR18]=contx(Arc, [gr3;gr4;gr1;gr2]);
[ZR19
ZR20]=contx(Arc, [circshift(gr3,4);circshift(gr4,4);circshift(gr1,4);circshift(gr2,4)]);
[ZR21
ZR22]=contx(Arc, [circshift(gr3,8);circshift(gr4,8);circshift(gr1,8);circshift(gr2,8)]);
[ZR23
ZR24]=contx(Arc, [circshift(gr3,12);circshift(gr4,12);circshift(gr1,12);circshift(gr2,12)]);

[ZR25 ZR26]=contx(Arc, [gr4;gr1;gr2;gr3]);
[ZR27
ZR28]=contx(Arc, [circshift(gr4,4);circshift(gr1,4);circshift(gr2,4);circshift(gr3,4)]);
[ZR29
ZR30]=contx(Arc, [circshift(gr4,8);circshift(gr1,8);circshift(gr2,8);circshift(gr3,8)]);
[ZR31
ZR32]=contx(Arc, [circshift(gr4,12);circshift(gr1,12);circshift(gr2,12);circshift(gr3,12)]);

A.4 CEQ²PSK system block diagram for Saha's Constellation.



Tsym= The duration of a Symbol
 Tsamp = Sampling Time
 fc= Frequency Carrier

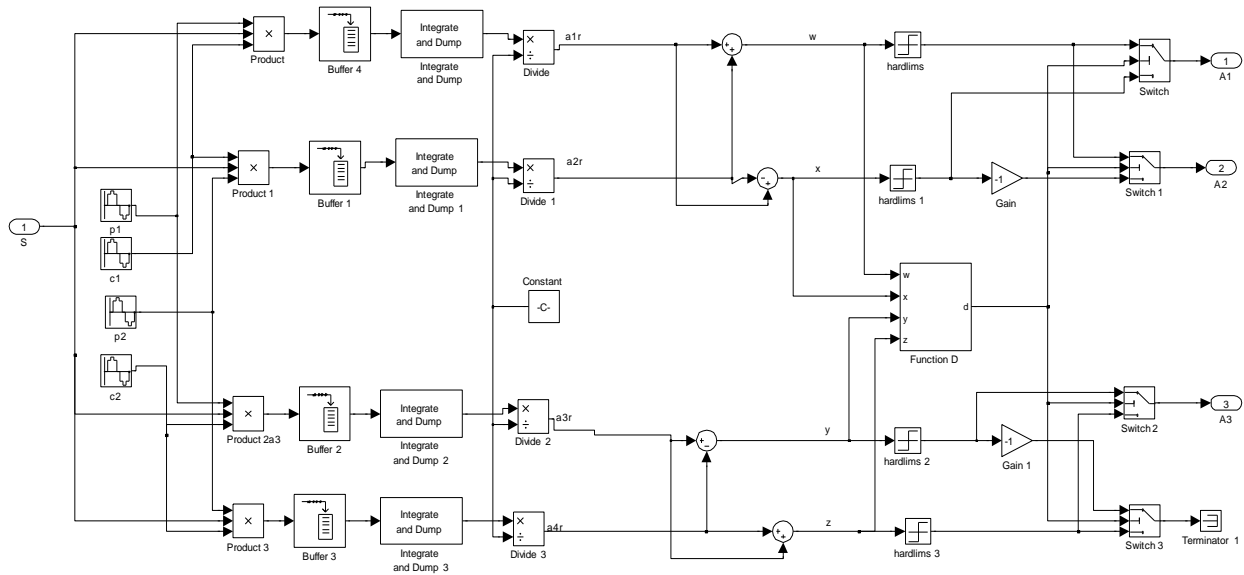
All these three parameters can be tuned in the model explorer
 Please click in View ->Model Explorer
 and then in the MODEL HERARCHY window please click on the Model Workspace
 Other wise you can set them up by
 using in matlab the command "setpar"

Eb/No range has to be set up in the workspace by using BER tool Box
 and the Max number of bits erros has to be set as well

BER variable name is "BER"

A.5 Optimal demodulator referenced in Chapter 3 for Saha's

Constellation.



A.6 Mapping by set-partitioning subroutine

```
function ys = fcn(indx,sub,setab,A1,A2,A3,A4,B1,B2,B3,B4)
% This block supports the Embedded MATLAB subset.
% See the help menu for details.
%-----
%-----
%All the subsets have 4 W groups of 256 points each, so in order to reach
%one of the 4 groups, the bits 9-10 are used to select the W groups inside
the
%the subsets. For instance let's have the subset A1=[W1 W2 W3 W4] that has
%1024 rows and 16 columns. Now if we want to select the group W2 we are going
%to need to move the indx of the row 257, and then add the integer that is
formed
%by the bits 1-8.
switch sub
    case 0
        pt=indx+1;
    case 1
        pt=indx+257;
    case 2
        pt=indx+513;
    case 3
        pt=indx+769;
    otherwise
        pt=1;
end
%-----
%-----

%Selection of the Subset
%-----
switch setab
    case 0
        ys=A1(pt,1:16)';
    case 4
        ys=A3(pt,1:16)';
    case 2
        ys=A2(pt,1:16)';
    case 6
        ys=A4(pt,1:16)';
    case 1
        ys=B1(pt,1:16)';
    case 5
        ys=B3(pt,1:16)';
    case 3
        ys=B2(pt,1:16)';
    case 7
        ys=B4(pt,1:16)';
    otherwise
        ys=zeros(1,16)';
end
%-----
```

A.7 Branch metric calculation embedded function

```

function [r5,r6,r7,r8] =Carsbd(c,B1,B2,B3,B4)
% This block supports the Embedded MATLAB subset.
% See the help menu for details.
%-----
%-----
eml.extrinsic('find'); %Declaring extrinsic function for this block.

%The following lines of code perform a lookup table

%-----
%-----Cartwright Signal-----
%-----Calculation of the squared distances-----
r5=zeros(1,3);
r6=r5; r7=r5; r8=r5;

%-----Convert signal received into a matrix of 1024X16-----
d=ones(1024,1);
f=d*c';
%-----

%-----
m1=sum((B1-f).^2,2);
r5(1)=min(m1);
i=find(m1==r5(1));
dummy1=0;
dummy1=max(i);
l=fix(dummy1/256);
wc=1*(l>0) - (dummy1==256) - (dummy1==512) - (dummy1==768) - (dummy1==1024);
k=mod(dummy1,256)-1; % the other 10 bits
indxc=k*(k>0)+(255*(k<0));
r5(2)=indxc;
r5(3)=wc;
%-----
m2=sum((B2-f).^2,2);
r6(1)=min(m2);
i=find(m2==r6(1));
dummy1=0;
dummy1=max(i);
l=fix(dummy1/256);
wc=1*(l>0) - (dummy1==256) - (dummy1==512) - (dummy1==768) - (dummy1==1024);
k=mod(dummy1,256)-1; % the other 10 bits
indxc=k*(k>0)+(255*(k<0));
r6(2)=indxc;
r6(3)=wc;
%-----
m3=sum((B3-f).^2,2);
r7(1)=min(m3);
i=find(m3==r7(1));
dummy1=0;
dummy1=max(i);
l=fix(dummy1/256);
wc=1*(l>0) - (dummy1==256) - (dummy1==512) - (dummy1==768) - (dummy1==1024);

```

```

k=mod(dummy1,256)-1;           % the other 10 bits
indxk=k*(k>0)+(255*(k<0));
r7(2)=indxk;
r7(3)=wc;
%-----
m4=sum((B4-f).^2,2);
r8(1)=min(m4);
i=find(m4==r8(1));
dummy1=0;
dummy1=max(i);
l=fix(dummy1/256);
wc=1*(l>0)-(dummy1==256)-(dummy1==512)-(dummy1==768)-(dummy1==1024);
k=mod(dummy1,256)-1;           % the other 10 bits
indxk=k*(k>0)+(255*(k<0));
r8(2)=indxk;
r8(3)=wc;
%-----

```

A.8 Add compare and select subroutine ('fcn').

```

function [bs0,bs1,bs2,bs3,bs4,bs5,bs6,bs7,pa,t,signa,wc,subset,bcot,ps2]=
fcn(s0,s1,s2,s3,s4,s5,s6,s7,r1,r2,r3,r4,r5,r6,r7,r8,cot,ps1)
% This block supports the Embedded MATLAB subset.
% See the help menu for details.
eml.extrinsic('find'); %Declaring extrinsic function for this block.

bcot=cot+1; %memory shift register counter

%----- Possible States at t=k, t=k+1-----
-----
a=ps1;
if ps1(1)==0||ps1(3)==2||ps1(5)==4||ps1(7)==6
    a(1)=0;
    a(2)=1;
    a(3)=2;
    a(4)=3;
end

if ps1(2)==1||ps1(4)==3||ps1(6)==5||ps1(8)==7
    a(5)=4;
    a(6)=5;
    a(7)=6;
    a(8)=7;
end
ps2=a;
%-----
-----

%-----Metric calculation for state k+1 according to the possible input
states-----
%-----Survivors are also determined in this lines of code-----
-----

```

```

%dummy variable has dummy(1,i)=metric dummy(2,i)=state before dummy(3,i)=

%-----State0 k+1-----
-----
dummy=[inf 0 0 r1(2:3);inf 2 1 r2(2) r2(3);inf 4 2 r3(2) r3(3);inf 6 3 r4(2)
r4(3)];
if ps1(1)==0
    dummy(1,1)=r1(1)+s0;
end
if ps1(3)==2
    dummy(2,1)=r2(1)+s2;
end
if ps1(5)==4
    dummy(3,1)=r3(1)+s4;
end
if ps1(7)==6
    dummy(4,1)=r4(1)+s6;
end

%-----Compare and select the best path comming to the state0 at time
k+1
m=[dummy(1,1) dummy(2,1) dummy(3,1) dummy(4,1)];
bs0=min(m);
%-----

%find signal in the survivor path of the state0 at k+1 time
i=find(m==bs0);
idx=0;
idx=max(i);
t0=dummy(idx,2);
su0=dummy(idx,3);
si0=dummy(idx,4);
w0=dummy(idx,5);
%-----

%-----State1 k+1-----
-----
dummy=[inf 0 1 r2(2) r2(3);inf 2 0 r1(2) r1(3);inf 4 3 r4(2) r4(3);inf 6 2
r3(2) r3(3)];
if ps1(1)==0
    dummy(1,1)=r2(1)+s0;
end
if ps1(3)==2
    dummy(2,1)=r1(1)+s2;
end
if ps1(5)==4
    dummy(3,1)=r4(1)+s4;
end
if ps1(7)==6
    dummy(4,1)=r3(1)+s6;
end

```

```

%-----Compare and select the best path comming to the statel at time
k+1
m=[dummy(1,1) dummy(2,1) dummy(3,1) dummy(4,1)];
bs1=min(m);
%-----
%find signal in the survivor path of the state0 at k+1 time
i=0;
i=find(m==bs1);
idx=0;
idx=max(i);
t1=dummy(idx,2);
sul=dummy(idx,3);
sil=dummy(idx,4);
w1=dummy(idx,5);
%-----State2 k+1-----
-----
dummy=[inf 0 2 r3(2) r3(3);inf 2 3 r4(2) r4(3);inf 4 0 r1(2) r1(3);inf 6 1
r2(2) r2(3)];
if ps1(1)==0
    dummy(1,1)=r3(1)+s0;
end
if ps1(3)==2
    dummy(2,1)=r4(1)+s2;
end
if ps1(5)==4
    dummy(3,1)=r1(1)+s4;
end
if ps1(7)==6
    dummy(4,1)=r2(1)+s6;
end
%-----Compare and select the best path comming to the state2 at time
k+1
m=[dummy(1,1) dummy(2,1) dummy(3,1) dummy(4,1)];
bs2=min(m);
%-----
%find signal in the survivor path of the state0 at k+1 time
i=0;
i=find(m==bs2);
idx=0;
idx=max(i);
t2=dummy(idx,2);
su2=dummy(idx,3);
si2=dummy(idx,4);
w2=dummy(idx,5);
%-----State3 k+1-----
-----
dummy=[inf 0 3 r4(2:3);inf 2 2 r3(2:3);inf 4 1 r2(2:3);inf 6 0 r1(2:3)];
if ps1(1)==0
    dummy(1,1)=r4(1)+s0;
end
if ps1(3)==2
    dummy(2,1)=r3(1)+s2;
end
if ps1(5)==4

```

```

    dummy(3,1)=r2(1)+s4;
end
if ps1(7)==6
    dummy(4,1)=r1(1)+s6;
end
%-----Compare and select the best path comming to the state3 at time
k+1
m=[dummy(1,1) dummy(2,1) dummy(3,1) dummy(4,1)];
bs3=min(m);
%-----
%find signal in the survivor path of the state3 at k+1 time
i=0;
i=find(m==bs3);
idx=0;
idx=max(i);
t3=dummy(idx,2);
su3=dummy(idx,3);
si3=dummy(idx,4);
w3=dummy(idx,5);
%-----State4 k+1-----
----
dummy=[inf 1 0 r5(2:3);inf 3 1 r6(2:3);inf 5 2 r7(2:3);inf 7 3 r8(2:3)];
if ps1(2)==1
    dummy(1,1)=r5(1)+s1;
end
if ps1(4)==3
    dummy(2,1)=r6(1)+s3;
end
if ps1(6)==5
    dummy(3,1)=r7(1)+s5;
end
if ps1(8)==7
    dummy(4,1)=r8(1)+s7;
end
%-----Compare and select the best path comming to the state4 at time
k+1
m=[dummy(1,1) dummy(2,1) dummy(3,1) dummy(4,1)];
bs4=min(m);
%-----
%find signal in the survivor path of the state4 at k+1 time
i=0;
i=find(m==bs4);
idx=0;
idx=max(i);
t4=dummy(idx,2);
su4=dummy(idx,3);
si4=dummy(idx,4);
w4=dummy(idx,5);
%-----State5 k+1-----
----
dummy=[inf 1 1 r6(2:3);inf 3 0 r5(2:3);inf 5 3 r8(2:3);inf 7 2 r7(2:3)];
if ps1(2)==1
    dummy(1,1)=r6(1)+s1;
end
if ps1(4)==3

```

```

    dummy(2,1)=r5(1)+s3;
end
if ps1(6)==5
    dummy(3,1)=r8(1)+s5;
end
if ps1(8)==7
    dummy(4,1)=r7(1)+s7;
end
%-----Compare and select the best path comming to the state5 at time
k+1
m=[dummy(1,1) dummy(2,1) dummy(3,1) dummy(4,1)];
bs5=min(m);
%-----
%find signal in the survivor path of the state4 at k+1 time
i=0;
i=find(m==bs5);
idx=0;
idx=max(i);
t5=dummy(idx,2);
su5=dummy(idx,3);
si5=dummy(idx,4);
w5=dummy(idx,5);
%-----

%-----State6 k+1-----
dummy=[inf 1 2 r7(2:3);inf 3 3 r8(2:3);inf 5 0 r5(2:3);inf 7 1 r6(2:3)];
if ps1(2)==1
    dummy(1,1)=r7(1)+s1;
end
if ps1(4)==3
    dummy(2,1)=r8(1)+s3;
end
if ps1(6)==5
    dummy(3,1)=r5(1)+s5;
end
if ps1(8)==7
    dummy(4,1)=r6(1)+s7;
end
%-----Compare and select the best path comming to the state6 at time
k+1
m=[dummy(1,1) dummy(2,1) dummy(3,1) dummy(4,1)];
bs6=min(m);
%-----
%find signal in the survivor path of the state4 at k+1 time
i=0;
i=find(m==bs6);
idx=0;
idx=max(i);
t6=dummy(idx,2);
su6=dummy(idx,3);
si6=dummy(idx,4);

```



```

w6=dummy(idx,5);
%-----
-----

%-----State7 k+1-----
-----
dummy=[inf 1 3 r8(2:3);inf 3 2 r7(2:3);inf 5 1 r6(2:3);inf 7 0 r5(2:3)];
if ps1(2)==1
    dummy(1)=r8(1)+s1;
end
if ps1(4)==3
    dummy(2)=r7(1)+s3;
end
if ps1(6)==5
    dummy(3)=r6(1)+s5;
end
if ps1(8)==7
    dummy(4)=r5(1)+s7;
end
%-----Compare and select the best path comming to the state7 at time
k+1
m=[dummy(1,1) dummy(2,1) dummy(3,1) dummy(4,1)];
bs7=min(m);
%-----
-----
%find signal in the survivor path of the state4 at k+1 time
i=0;
i=find(m==bs7);
idx=0;
idx=max(i);
t7=dummy(idx,2);
su7=dummy(idx,3);
si7=dummy(idx,4);
w7=dummy(idx,5);
%-----
-----

pa=[bs0;bs1;bs2;bs3;bs4;bs5;bs6;bs7];
t=[t0;t1;t2;t3;t4;t5;t6;t7];
subset=[su0;su1;su2;su3;su4;su5;su6;su7];
signa=[si0;si1;si2;si3;si4;si5;si6;si7];
wc=[w0;w1;w2;w3;w4;w5;w6;w7];
%-----counter for decision-----
%-----Initialization parameters-----
if bcot<=2
    ps2=[0;0;0;0;0;0;0;0];
    bs0=0;
    bs1=0;
    bs2=0;
    bs3=0;
    bs4=0;
    bs5=0;
    bs6=0;
    bs7=0;
    t=[0;0;0;0;0;0;0;0];

```

```

subset=t;
end

```

A.9 Trace-back Function

```

function [t0,t1,t2,t3,t4,t5,t6,t7,d,I0,I1,I2,I3,I4,I5,I6,I7]=
traceback(q0,q1,q2,q3,q4,q5,q6,q7,pa,u,signa,w,v,c1)
% This block supports the Embedded MATLAB subset.
% See the help menu for details.
%U is a matrix of constraint length by number of states

indx=u+1; %Conversion of state to Index
y0=zeros(1,c1);
y1=y0;y2=y0;y3=y0;y4=y0;y5=y0;y6=y0;y7=y0;
x0=zeros(1,c1);
x1=x0;x2=x0;x3=x0;x4=x0;x5=x0;x6=x0;x7=x0;
z0=zeros(1,c1);
z1=z0;z2=z0;z3=z0;z4=z0;z5=z0;z6=z0;z7=z0;

j0=1;
j1=j0+1;j2=j0+2;j3=j0+3;j4=j0+4;
j5=j0+5;j6=j0+6;j7=j0+7;
for i=1:1:c1
    %Trace back eight possible paths
    y0(c1+1-i)=v(c1+1-i,j0);
    y1(c1+1-i)=v(c1+1-i,j1);
    y2(c1+1-i)=v(c1+1-i,j2);
    y3(c1+1-i)=v(c1+1-i,j3);
    y4(c1+1-i)=v(c1+1-i,j4);
    y5(c1+1-i)=v(c1+1-i,j5);
    y6(c1+1-i)=v(c1+1-i,j6);
    y7(c1+1-i)=v(c1+1-i,j7);

    x0(c1+1-i)=signa(c1+1-i,j0);
    x1(c1+1-i)=signa(c1+1-i,j1);
    x2(c1+1-i)=signa(c1+1-i,j2);
    x3(c1+1-i)=signa(c1+1-i,j3);
    x4(c1+1-i)=signa(c1+1-i,j4);
    x5(c1+1-i)=signa(c1+1-i,j5);
    x6(c1+1-i)=signa(c1+1-i,j6);
    x7(c1+1-i)=signa(c1+1-i,j7);

    z0(c1+1-i)=w(c1+1-i,j0);
    z1(c1+1-i)=w(c1+1-i,j1);
    z2(c1+1-i)=w(c1+1-i,j2);
    z3(c1+1-i)=w(c1+1-i,j3);
    z4(c1+1-i)=w(c1+1-i,j4);
    z5(c1+1-i)=w(c1+1-i,j5);
    z6(c1+1-i)=w(c1+1-i,j6);

```

```

z7(c1+1-i)=w(c1+1-i,j7);

j0=indx(c1+1-i,j0);
j1=indx(c1+1-i,j1);
j2=indx(c1+1-i,j2);
j3=indx(c1+1-i,j3);
j4=indx(c1+1-i,j4);
j5=indx(c1+1-i,j5);
j6=indx(c1+1-i,j6);
j7=indx(c1+1-i,j7);
end



```

%preparing variable for decision
%X values stored the 8 first bits, Y values stored 2 last bits
I0=[x0(1) z0(1) y0(1)]; I1=[x1(1) z1(1) y1(1)]; I2=[x2(1) z2(1) y2(1)];
I3=[x3(1) z3(1) y3(1)];
I4=[x4(1) z4(1) y4(1)]; I5=[x5(1) z5(1) y5(1)]; I6=[x6(1) z6(1) y6(1)];
I7=[x7(1) z7(1) y7(1)];

%forgetting some paths
r=zeros(1,8);
r=pa(c1,:);
t0=r(1); t1=r(2); t2=r(3); t3=r(4);
t4=r(5); t5=r(6); t6=r(7); t7=r(8);
d=r;
r(1)=r(1)-q0; r(2)=r(2)-q1; r(3)=r(3)-q2; r(4)=r(4)-q3;
r(5)=r(5)-q4; r(6)=r(6)-q5; r(7)=r(7)-q6; r(8)=r(8)-q7;

```


```

A.10: Contained in the attached CD

Simulink Models, Spread Sheets of the partitions, Matalab Variables, Matlab subroutines.

A.11: Co-author permission letters

April 8, 2009

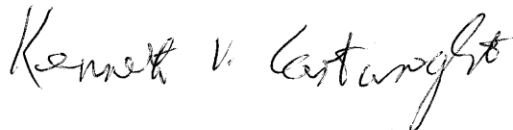
Milton I. Quinteros
Department of Electrical Engineering
EN 616A Lakefront Campus
University of New Orleans
New Orleans, LA 70148, U.S.A.

Dear Mr. Quinteros,

As a co-author on two conference papers that appear as two chapters of your Master's Thesis, I authorize you to use the portions of the chapters to which I contributed. I acknowledge that you were the first author on the IEEE Region 5 BASICS paper (2008) and also on the 2009 paper submitted to IEEE Globecom'09.

If you have any questions, I may be contacted at kvc@batelnet.bs.

Sincerely,



Dr. Kenneth V. Cartwright

April 8, 2009

Milton I. Quinteros
Department of Electrical Engineering
EN 616A Lakefront Campus
University of New Orleans
New Orleans, LA 70148, U.S.A.

Dear Mr. Quinteros,

As a co-author on one conference paper that appears as one chapter of your Master's Thesis, I authorize you to use the portions of the chapter to which I contributed. I acknowledge that you were the first author on the IEEE Region 5 BASICS paper (2008).

If you have any questions, I may be contacted at urgalleg@uno.edu.

Sincerely,

Ricardo Gallegos
Student ID # 2233235

Ricardo Gallegos

Vita

Milton Quinteros was born on August 4, 1982, in Guayaquil, Ecuador. He received a Bachelor of Science in Electrical Engineering from the University of New Orleans in May 2007 and began working on his Master of Science in Electrical Engineering in August 2007. He has worked at the Intensive English Language Program (IELP) as student worker where he designed a data base for this program. In addition, he worked as a Research Assistant in Electrical Engineering under Dr. Edit J. Kaminsky Bourgeois. His research areas include Digital Telecommunications, Data Base, Neural Networks, and Digital System Controls. He plans to enter the Ph. D. Program in Engineering and Applied Science at UNO after receiving his Master's degree.